GSFC TDMS CMO
<Date>
Released

47x-xxxxx, Revision -
QuickSounder (QS) Flight Project, Code 472

QS ATMS Calibration Data Book
Government Version
Pre-Launch Version

2026-08-15

APPROVED FOR PUBLIC RELEASE

Goddard Space Flight Center
Greenbelt, Maryland

QUICKSOUNDER

NOAA / NASA

QuickSounder/QS ATMS Calibration Data Book

Government Version

Review/Signature/Approval Page

Prepared by:

Dr. ChengHsuan Lyu

GSFC/NASA/Morgan State University

Approved by:

TBD

Electronic Approval available on-line at: https:// ipdtdms.gsfc.nasa.gov/frontmenu_dsp.cfm

Preface

This document is under the Technical Data Management System (TDMS) Program/Flight configuration control. Once this document is approved, TDMS approved changes are handled in accordance with Class I and Class II change control requirements as described in the Technical Data Management System Configuration Management Procedures, and changes to this document shall be made by complete revision.

Any questions should be addressed to:

The TDMS Configuration Management Office
NASA/GSFC
Code 472
Greenbelt, MD 20771

Change History Log

Revision	Effective Date	Description of Changes
-	TBD	Initial release per 47x-CCR-xx-xxxx.

Table of TBDs/TBRs/TBSs

Item No.	Location	Summary	Individual Org.	Due Date or Event
1	Sec. 5.2	Antenna Beam Pointing Offset Data	NASA	Post Sat TVAC
2	Sec. 5.3	Antenna Flat Reflector Emissivity	NASA	Post Launch
3	Sec. 6.4	Warm load temperature error correction	NASA	Post Launch
4	Sec. 7.2	Lunar Intrusion Correction	NASA	Post Launch
5	Sec. 8.1.2	On-orbit 300 K NEDT	MIT-LL	Post Launch
6	Sec. 11	QS On-orbit dG/G & 1/f	NASA	Post-Launch
7	Sec. 12	STRIPING INDEX	NOAA	Post Launch
8	Sec. 13	ON-ORBIT PROCESSING PCT TABLES	NOAA	Post Launch
9	Sec. 14	ICVS WEBSITE AND SERVICES	NOAA	Post Launch

Table of Contents

List of Figures

List of Tables

1. SCOPE

The Advanced Technology Microwave Sounder (ATMS) SN301 is an instrument onboard the QuickSounder Satellite System, QuickSounder mission (renamed QS). Throughout this document the mission may be referred to as QuickSounder or QS. The purpose of this document is to provide information needed to interpret and process QS ATMS science data.

The contents of the data book incorporate results from pre-launch subsystem-level and instrument-level testing as well as post-launch testing performed during instrument commissioning. Major milestones include instrument thermal vacuum (TVAC) testing in May 2024 and observatory TVAC testing in 2026. QS launch will be no earlier than Feb. 15, 2027.

2. INTRODUCTION

2.1 ATMS Design

ATMS was designed and built for NASA by Northrop Grumman Corporation in Azusa, California.

ATMS is the passive 22-channel microwave sounder for the QS program, operating in a polar sun-synchronous low Earth orbit. The ATMS measures emitted atmospheric radiation in five frequency bands, centered at 23.80 GHz (K band), 31.40 GHz (Ka band), 50.30-57.29 GHz (V band), 88.20 GHz (W band), 165.50 GHz, and 183.31 GHz (G band). The receivers for the five bands are assembled into four receiver "shelves" – the K/Ka-band receiver shelf, V-band receiver shelf, W-band receiver shelf, and G-band receiver shelf.

The ATMS is a total-power radiometer, with "through-the-antenna" radiometric calibration, meaning the on-orbit calibration utilizes calibration reference energy measured through the antennas, providing end-to-end calibration. Radiometric data is collected by two antenna apertures, scanned by rotating flat-plate reflectors. Scanning is performed perpendicular to the satellite motion, from sun to anti-sun, using the "integrate-while-scan" type data collection. The main characteristics of the ATMS instrument are listed in Table 2.1.

Table 2.1: ATMS Instrument Characteristics in Design Attribute

Ch	Channel Central Freq. (MHz)	Polarization	Bandwidth Max. (MHz)	Frequency Stability (MHz)*	Calibration Accuracy (K)	NEΔT (K)	3-dB Beamwidth (deg)
1	23800	QV	270	< 10	1.0	0.70	5.2
2	31400	QV	180	< 10	1.0	0.80	5.2
3	50300	QH	180	< 10	0.75	0.90	2.2
4	51760	QH	400	< 5	0.75	0.70	2.2
5	52800	QH	400	≤ 5	0.75	0.70	2.2
6	53596±115	QH	170	≤ 5	0.75	0.70	2.2
7	54400	QH	400	≤ 5	0.75	0.70	2.2
8	54940	QH	400	≤ 10	0.75	0.70	2.2
9	55500	QH	330	≤ 10	0.75	0.70	2.2
10	57290.344(f_o)	QH	330	≤ 0.5	0.75	0.75	2.2
11	f_o± 217	QH	78	< 0.5	0.75	1.20	2.2
12	f_o±322.2±48	QH	36	< 1.2	0.75	1.20	2.2
13	f_o±322.2±22	QH	16	< 1.6	0.75	1.50	2.2
14	f_o±322.2±10	QH	8	< 0.5	0.75	2.40	2.2

Ch	Channel Central Freq. (MHz)	Polarization	Bandwidth Max. (MHz)	Frequency Stability (MHz)*	Calibration Accuracy (K)	NEΔT (K)	3-dB Beamwidth (deg)
15	f_o±322.2±4.5	QH	3	≤ 0.5	0.75	3.60	2.2
16	88200	QV	2000	≤ 200	1.0	0.50	2.2
17	165500	QH	3000	≤ 200	1.0	0.60	1.1
18	183310±7000	QH	2000	≤ 30	1.0	0.80	1.1
19	183310±4500	QH	2000	≤ 30	1.0	0.80	1.1
20	183310±3000	QH	1000	≤ 30	1.0	0.80	1.1
21	183310±1800	QH	1000	< 30	1.0	0.80	1.1
22	183310±1000	QH	500	< 30	1.0	0.90	1.1

Note: QV stands for Quasi-V and QH stands for Quasi-H, see Figure 2-2 below. * Requirement for JPSS-2 ATMS, but not for QS

QS ATMS has two receiving antenna apertures, with one aperture serving for channels 1-15 with frequencies below 60 GHz and a separate aperture for channels 16-22 with frequencies above 60 GHz. As shown in Figure 2-1, the antenna subsystems consist of a flat plate reflector mounted on a scan axis at a 45° tilt angle so that radiation is reflected from a direction perpendicular to the scan axis into a direction along the scan axis (i.e., a 90° reflection). With the scan axis oriented in the along-track direction, i.e., the spacecraft velocity direction, this results in a cross-track scan pattern. Note that the green line connecting to the rotating reflectors is the scan axis. The reflected radiation is focused by a stationary (fixed) parabolic reflector onto a polarizing grid, which either reflects or passes the radiation to a feedhorn.

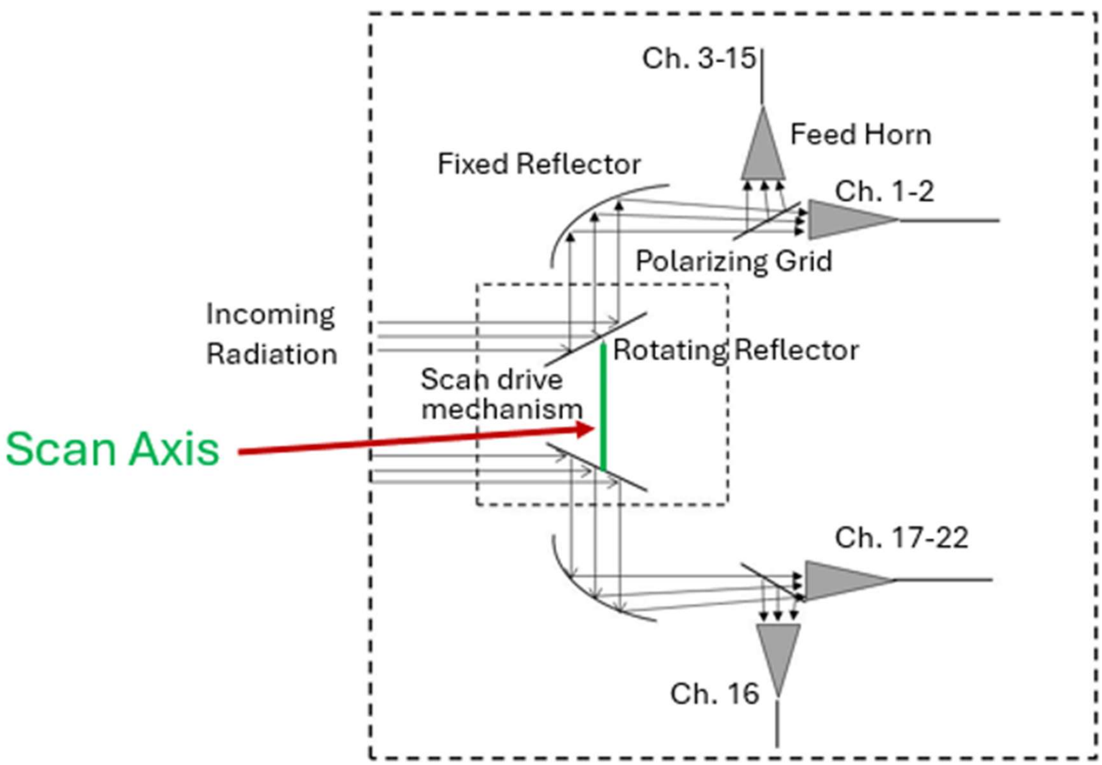

Figure 2-1: **Schematic diagram of ATMS antenna subsystem**

The top portion shows the antenna subsystem for K/Ka and V bands whereas the lower portion is for W/G bands.

The ATMS scan mechanism is synchronized to the spacecraft clock with a synchronization pulse every 8 seconds (i.e. for every third revolution). The antenna reflectors rotate continuously, yet not constant velocity in normal operational scan, completing three revolutions in 8 seconds. See Figure 2.2 below, each scan cycle is divided into three viewing segments, comprising a view of the Earth scene and two calibration references scenes, across 104 beam positions (BPs). In the first segment the earth is viewed at 96 different angles, symmetric around the nadir direction. The antenna is in continuous motion, and the 96 samples are taken "on the fly", with each sample representing the mid-point of a brief sampling interval of about 17.660 *ms*. The scan speed is such that the corresponding angular sampling interval is 1.11°, i.e., the scan speed is about 61.6°/second. The antenna then accelerates and moves to a position that points toward an unobstructed view of space, i.e., between the earth's limb and the spacecraft horizon. There it resumes the same slow scan speed as maintained across the Earth scenes while four consecutive cold calibration measurements are taken. Next, the antenna is again accelerated to the zenith direction, which points it toward an internal calibration target that is at the relatively high ambient instrument temperature and is again slowed down to normal scan speed while four consecutive warm calibration measurements are taken. Finally, it is accelerated to the starting Earth scene position, where it is slowed down to normal scan speed to begin another scan cycle. Note that in this document the terms "warm cal", "warm target", "warm load", "hot target", or "blackbody target" all refer to the ATMS internal calibration target (ICT) unless otherwise noted.

Figure 2-2, together with Figure 2-1, shows also how the polarized scene radiation is reflected by the scanning flat reflector mirror and the definition of polarization status of ATMS observations.

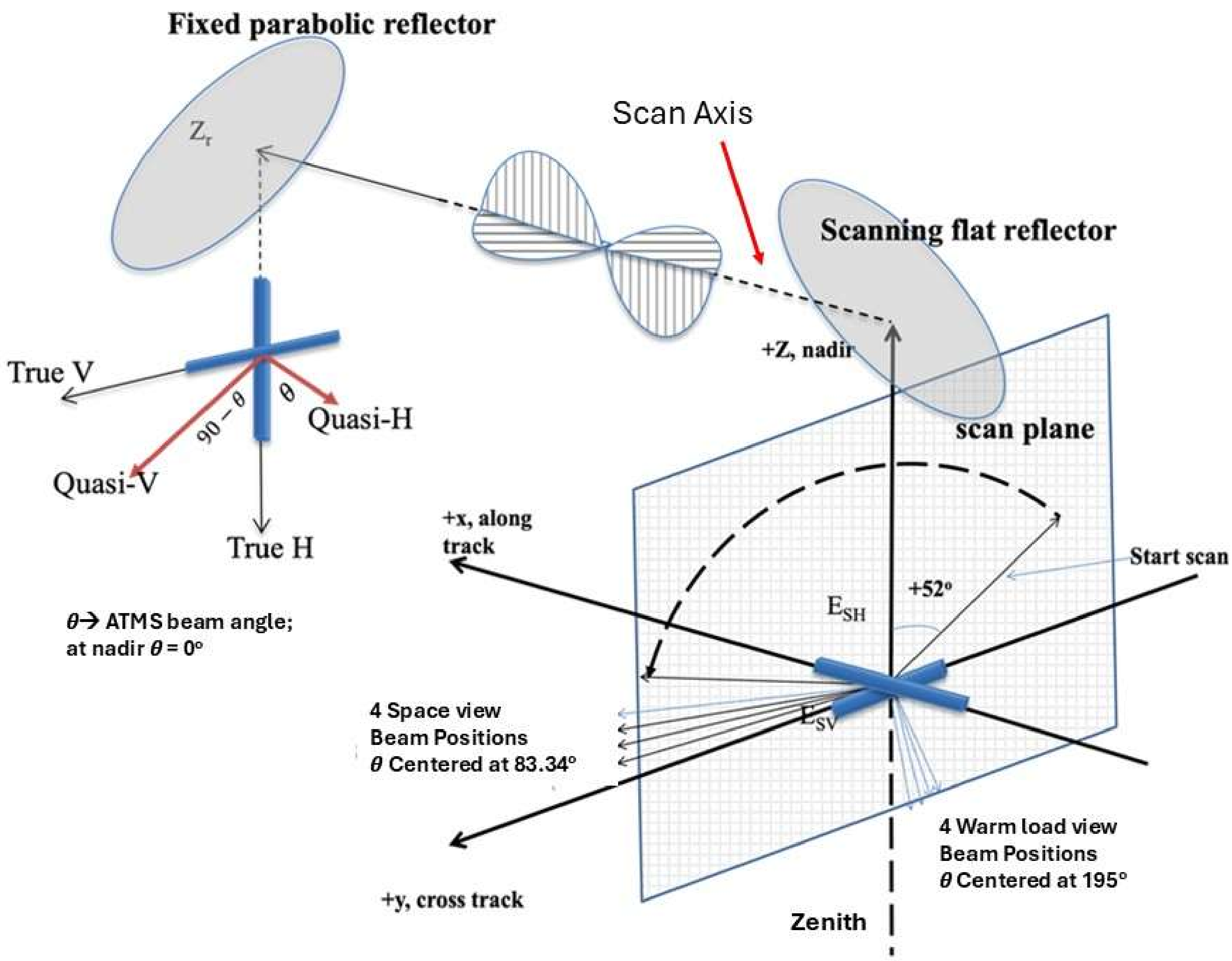

Figure 2-2: **Sketch plot for polarization direction definition by taking scene incident plane as reference frame**

Note SV (Space View) scan position is sketched for ATMS scan profile #1, space view centered at 83.34°, not to scale.

For QS ATMS, the term "Quasi-V (QV)" or "Quasi-vertical" indicates that while the polarization is intended to be vertical relative to the Earth's surface at nadir, its actual orientation changes slightly as the instrument scans away from nadir due to the viewing geometry. The vertical polarization is the component whose electric field is lying in the plane of incidence, and the horizontal polarization is the component whose electrical field is perpendicular to the plane of incidence. Note the plane of incidence is the same as the scan plane. When the reflector scans to an angle of θ relative to the feed horn orientation, the received antenna brightness temperature is a combination of the vertical and horizontal components.

For ATMS channels 1, 2 and 16, the observed brightness temperature is in QV polarization, which can be expressed as a function of brightness temperature in pure V polarization (TB_v) and pure H polarization (TB_h) as below:

$$TB_{QV} = TB_v \cdot \cos^2\theta + TB_h \cdot \sin^2\theta \qquad \text{Equation 2-1}$$

For ATMS channels 3 – 15, and 17 – 22, the observed brightness temperature is in Quasi-H (QH) polarization, which can be expressed as a function of brightness temperature in pure V polarization (TB_v) and pure H polarization (TB_h) as below:

$$TB_{QH} = TB_v \cdot \sin^2\theta + TB_h \cdot \cos^2\theta \qquad \text{Equation 2-2}$$

2.2 Radiance Calibration based on Planck Function

For microwave sounding instruments like ATMS, the radiance can be derived directly from the output counts by using the two-point linear calibration equation, due to the linearity correlation between the counts and the incoming radiation:

$$R = R_w + (R_w - R_c)\left(\frac{C_s - \overline{C_w}}{\overline{C_w} - \overline{C_c}}\right) + Q^R, \qquad \text{Equation 2-3}$$

where R_w and R_c are the warm and cold calibration target radiance corresponding respectively to the warm and cold target temperatures (T_w and T_c). The parameters $\overline{C_w}$ and $\overline{C_c}$ represent the mean warm and cold counts; C_s is the scene count; and Q^R is the calibration non-linearity correction term. As mentioned earlier, each of the two calibration targets - i.e., the warm load and cold space - is sampled four times in succession. The measurements are in the unit of digital "counts," which represent the radiometer's output. It is assumed that the radiative environment does not change between successive calibration samplings, so that any differences among the measurements are strictly due to noise. This noise can be reduced by averaging or smoothing the measurements.

In the current radiometric calibration algorithm, radiance is calculated from Planck's law as a function of frequency and the temperature:

$$R(\upsilon, T) = \frac{2h\upsilon^3}{c^2}\frac{1}{e^{\frac{h\upsilon}{kT}} - 1}. \qquad \text{Equation 2-4}$$

In the equation above, the Planck's constant, h, is $6.626070040 \times 10^{-34}\, J \cdot s$ and υ is frequency in Hz. Meanwhile, the speed of light, c, has a value of $2.99792458\, x10^8\, m/s$, the Boltzmann constant is given by $k = 1.38064853 \times 10^{-23} J/K$, and T is a physical temperature in units of K. The unit of radiance from this equation is $J \cdot s^{-1} \cdot m^{-2} \cdot sr^{-1} \cdot Hz^{-1}$.

In radiance calibration, the warm load calibration target and cosmic background brightness temperatures need to be transformed to radiance by using the Planck function. During the process, the spectral response functions (SRFs) for different ATMS receiver bands need to be considered when using these temperatures. For creating a functional relationship between antenna subsystem hardware spectral brightness temperature T, and band corrected brightness temperature, T', the band-integrated radiance R' is computed, based on receiver outputs, by integrating the product of spectral radiance $R(\nu,T)$ and spectral response function, $S(\nu)$, over the range of measured frequencies:

$$R' = \int_{\nu_1}^{\nu_2} R(\nu, T) S^n(\nu)\, d\nu \qquad \text{Equation 2-5}$$

$$= \int_{\nu_1}^{\nu_2} R(\nu, T) S(\nu)\, d\nu \Big/ \int_{\nu_1}^{\nu_2} S(\nu)\, d\nu$$

By using the equation above, the radiance was calculated for spectral brightness temperatures ranging from 2.73K to 330K using normalized receiver SRFs for each of the 22 ATMS channels. Note the SRF, $S^n(\nu)$, in the equation is already normalized against the total power integrated response over the frequency range.

In ATMS radiance calibration, the following equation is to apply the band correction for temperature in Equation 2-4 for radiance calculation.

$$Tb' = c_0 + c_1 \cdot Tb \qquad \text{Equation 2-6}$$

Since the primary ATMS antenna Temperature Data Record (TDR) and Sensor Data Record (SDR) product is brightness temperature in units of K, the retrieved radiance after correction needs to be converted to channel brightness temperature using the inverse Planck's Function:

$$Tb' = \frac{h \cdot \nu_0}{k \cdot ln\left(1 + \frac{2h\nu_0^3}{c^2 R'}\right)}, \qquad \text{Equation 2-7}$$

where ν_0 is the weighted mean center frequency of the measured SRF for each ATMS channel.

The band corrected brightness temperature in SDR can then be inverted from Equation 2-6 as:

$$Tb = \frac{1}{c_1} \cdot (Tb' - c_0) \qquad \text{Equation 2-8}$$

Note the other way to determine Tb is to use a table which contains Tb' and R' conversion table.
The center frequency and band correction coefficients for QS ATMS are listed in Table 2.2.

Table 2.2: Coefficients c_0 and c_1 calculated by using QS ATMS SRF measurements

Channel	Weighted Mean Center Frequency (Hz)	c_0 (K)	c_1
1	2.38018E+10	-0.00001565	1.00000931
2	3.14051E+10	-0.00000534	1.00000242
3	5.02990E+10	-0.00000423	1.00000122
4	5.17647E+10	-0.00001714	1.00000479
5	5.28023E+10	-0.00001632	1.00000448
6	5.36026E+10	-0.00002005	1.00000542
7	5.43974E+10	-0.00001544	1.00000412
8	5.49373E+10	-0.00001560	1.00000412
9	5.54997E+10	-0.00001074	1.00000281
10	5.72911E+10	-0.00001011	1.00000257
11	5.72902E+10	-0.00005739	1.00001455
12	5.72904E+10	-0.00013385	1.00003394
13	5.72918E+10	-0.00012587	1.00003192
14	5.72904E+10	-0.00012549	1.00003182
15	5.72914E+10	-0.00012324	1.00003125
16	8.82051E+10	-0.00029007	1.00004879
17	1.65508E+11	-0.00039214	1.00003667
18	1.83252E+11	-0.01855601	1.00146991
19	1.83252E+11	-0.00742450	1.00059380
20	1.83252E+11	-0.00329449	1.00026680

Channel	Weighted Mean Center Frequency (Hz)	c_0 (K)	c_1
21	1.83252E+11	-0.00113093	1.00009365
22	1.83252E+11	-0.00035357	1.00003019

2.3 Temperature Calibration based on Modified Rayleigh-Jeans Approximation

The Planck function Equation 2-4 is well modeled by the Rayleigh-Jeans approximation when $h\nu \ll kT$. This approximation is largely valid for ATMS frequencies and expected scene temperatures. It is given by the following equation

$$R(\nu, T) = \frac{2\nu^2 k}{c^2} T, \qquad \text{Equation 2-9}$$

where the terms are defined as in Equation 2-4. The Rayleigh-Jeans approximation to blackbody radiance is linear in physical temperature and therefore justifies a linear calibration equation in terms of brightness temperature. However, the approximation worsens at extremely cold temperatures coupled with high frequencies. This scenario occurs during the cold space calibration view at the higher frequency channels. It is therefore necessary to use a modified version of the Rayleigh-Jeans approximation to correct for brightness temperature errors.

To correct for the error in the Rayleigh-Jeans approximation at low temperatures and high frequencies, it is more appropriate to use the thermodynamic definition of brightness temperature, which is derived from a higher order approximation to the Planck function. First,

$$R(\nu, T_B) = \frac{2h\nu^3}{c^2}\left[e^{\frac{h\nu}{kT_B}} - 1\right]^{-1} \approx \frac{2h\nu^3}{c^2}\left[\frac{h\nu}{kT_B} + \frac{1}{2}\left(\frac{h\nu}{kT_B}\right)^2\right]^{-1} = \frac{2h\nu^3}{c^2}\frac{kT_B}{h\nu}\left[1 + \frac{1}{2}\frac{h\nu}{kT_B}\right]^{-1} \qquad \text{Equation 2-10}$$

since $e^{\frac{h\nu}{kT_B}} \approx 1 + \frac{h\nu}{kT_B} + \frac{1}{2}\left(\frac{h\nu}{kT_B}\right)^2$ for $\frac{h\nu}{kT_B} \ll 1$. Next,

$$\frac{2h\nu^3}{c^2}\frac{kT_B}{h\nu}\left[1 + \frac{1}{2}\frac{h\nu}{kT_B}\right]^{-1} \approx \frac{2h\nu^3}{c^2}\frac{kT_B}{h\nu}\left[1 - \frac{1}{2}\frac{h\nu}{kT_B}\right] = \frac{2h\nu^3}{c^2}\left[\frac{kT_B}{h\nu} - \frac{1}{2}\right] = \tilde{R}(\nu, T_B) \qquad \text{Equation 2-11}$$

since and $\frac{1}{1-x} \approx 1 + x$ for $x \ll 1$. Equating the approximation $\tilde{R}(\nu, T_B)$ to the Planck function $R(\nu, T_k)$ and solving for brightness temperature results in the following equation for thermodynamic brightness temperature

$$T_B = \frac{h\nu}{k}\left[\left(e^{\frac{h\nu}{kT_k}} - 1\right)^{-1} + \frac{1}{2}\right] \qquad \text{Equation 2-12}$$

where T_k is the kinetic (physical) temperature of the scene.

The brightness temperature calibration equation is given by

$$T = T_w + (T_w - T_c)\left(\frac{C_s - \overline{C_w}}{\overline{C_w} - \overline{C_c}}\right) + Q^T \qquad \text{Equation 2-13}$$

where T_w and T_c are the warm and cold calibration target brightness temperatures given by Equation 2-12 and the remaining terms are as in Equation 2-3, however, there is a change in units in Q terms, as denoted by superscript T and R. Q^T is in units of Kelvin and Q^R is in units of $J \cdot s^{-1} \cdot m^{-2} \cdot sr^{-1} \cdot Hz^{-1}$.

To compensate for the error introduced by the modified Rayleigh-Jeans approximation, an additional term is added to the cold calibration temperature such that the resulting linear calibration curve passes through the true brightness temperature at the mid-scene temperature. The correction term is given by

$$\Delta T_{RJ} = (T_c^{RJ} - T_c) - (T_m^{RJ} - T_m) \quad \text{Equation 2-14}$$

where T_c^{RJ} is the brightness temperature given by Equation 2-12 for the cold space physical temperature $T_c =$ 2.73 K and T_m^{RJ} is the brightness temperature for mid-scene physical temperature T_m at each channel. The correction terms (ΔT_{RJ}) and mid-scene temperatures for each channel are listed in Table 2.3.

Table 2.3: Cosmic Background Rayleigh-Jeans Corrections

Channel	Center Frequency (Hz)	Mid-Scene Temperature (K)	ΔT_{RJ} (K)
1	2.38E+10	190.0	0.039
2	3.14E+10	190.0	0.068
3	5.03E+10	227.5	0.174
4	5.18E+10	227.5	0.184
5	5.28E+10	227.5	0.191
6	5.36E+10	227.5	0.197
7	5.44E+10	227.5	0.203
8	5.49E+10	227.5	0.207
9	5.55E+10	227.5	0.211
10	5.73E+10	227.5	0.224
11	5.73E+10	227.5	0.224
12	5.73E+10	227.5	0.224
13	5.73E+10	227.5	0.224
14	5.73E+10	227.5	0.224
15	5.73E+10	227.5	0.224
16	8.82E+10	230.0	0.520
17	1.66E+11	260.0	1.680
18	1.83E+11	260.0	2.010
19	1.83E+11	260.0	2.010
20	1.83E+11	260.0	2.010
21	1.83E+11	260.0	2.010
22	1.83E+11	260.0	2.010

2.4 Additional ATMS Information

Additional introduction can be found in Appendix A. It mentioned two features of Near Earth Orbit Network (NEON) QS mission. First, it shows QS ATMS scanning ground swath and footprint geometry. Second, it shows 2027 planned on-orbit NEON & JPSS constellation configuration of QS, JPSS-2 (NOAA-21), JPSS-1 (NOAA-20), and S-NPP.

3. PRT SENSOR AND OTHER ENGINEERING DATA

Platinum resistance temperature sensors (PRTs) are used throughout the instrument to monitor key temperatures. These sensors each have unique coefficients based on the manufacturer's data; the coefficients for all QS-ATMS PRTs are provided in Section 3.1 to 3.3 of this document.

A PRT has a resistance that is a known function of temperature. There are two steps to convert a PRT raw count to a corresponding physical temperature. The signal from each PRT is digitized via an A-to-D converter aboard the ATMS instrument, which provides a count from 0 to 65,535 representing the resistance of a given PRT. The first step is to convert the count to resistance, given by the following equation 3-1, which includes parameters and the packet Word location of the parameter, can be found in Table 3.1 below:

$$R = \frac{\gamma_R}{\gamma_1 - \gamma_0}[C - \gamma_0] \text{ - Rc}$$

Equation 3-1

Where:
C = number of digital counts measured for the PRT at the output of the A-to-D converter
Rc = resistance of cable to the PRT (applicable only to 2-wire PRTs)
γ_R, γ_0, and γ_1 = parameters defined in Table 3.1

Table 3.1: PRT Counts Conversion Parameters

Parameter	4-Wire PRTs & Shelf PRTs		2-Wire PRTs	
	Mnemonic	**Word #**	**Mnemonic**	**Word #**
γ_R	PAM_REST_KAV or PAM_REST_WG, in Ohms	Word #1 or #2 of Calibration Packet	MUXREST1_A MUXREST2_A MUXREST1_B MUXREST2_B Housekeeping reference resistance, in Ohms	Words #212- 215 of Calibration Packet
γ_0	4W_GND, in Counts	Word #46 of LEO&A, Housekeeping, and Engineering Housekeeping Packet	2W_GND, in Counts	Word #47 of LEO&A, Housekeeping, and Engineering Housekeeping Packet
γ_1	KAV_WL_4WRES or WG_WL_4WRES, in Counts	Word #9 or #17 of Engineering Hot Calibration Packet	HK_2WREST1 or HK_2WREST2, in Counts	Words #44 and #45 of LEO&A, Housekeeping, and Engineering Housekeeping Packet

After computing the resistance, R, the second step is to use the Callendar Van Dusen equation to determine the physical temperature of each PRT. The equation is given below:

$$R = R_0\left[1+\alpha\left(T-\delta\left(\frac{T}{100}-1\right)\left(\frac{T}{100}\right)-\beta\left(\frac{T}{100}-1\right)\left(\frac{T}{100}\right)^3\right)\right]$$ Equation 3-2

Where:

T = physical temperature of the PRT in units of Celsius
R = resistance (ohms) of the PRT (from equation 3-1)
R_o = resistance at ice point of the PRT (supplied by PRT vendor)
α, δ, β = constant measured for the PRT (supplied by PRT vendor)

For the 4-wire PRTs, the Newton-Raphson technique can be used to perform the inversion, to compute T for a given R. If one solves for T by putting equation 3-2 in a polynomial format with respect to T and the corresponding coefficients, the polynomial coefficients can be put in vector form into a solver such as MATLAB's roots() function to estimate T within roundoff error. This requires an initial guess for the iterative process and setting an iteration limit. For the first guess, use equation 3-3, or the subsequent Equation 3-4, as the limit.

$$T = \frac{R-\text{Ro}}{\text{Ro}\,\alpha}$$ Equation 3-3

Note that the best solution is to solve equation 3-2 using roots, then select the root value closest to the first guess. It would then require no iteration.

3.1 Warm Target 4-Wire PRTs

To support the processing of the 4-wire PRTs as described above, the following coefficients are provided in data words 3-62 in the Calibration Data Packet: R_0, α, δ, β. Table 3.2 and Table 3.3 list these coefficients for the KAV warm targets PRTs and WG warm target PRTs, respectively.

Table 3.2: Coefficients for KAV Warm Target 4-Wire PRTs

KAV PRT	R_0 [Ω]	α [°C^{-1}]	δ [°C]	β [°C]
1	1998.572101	0.00385219	1.68947	0.37231
2	1996.527371	0.00385697	1.68547	-0.10265
3	1998.845355	0.00385354	1.68073	0.48746
4	1998.752765	0.00385413	1.69027	-0.02979
5	1999.097497	0.00385424	1.68623	0.20707
6	1998.145157	0.00385316	1.68475	-0.23494
7	1998.898639	0.00385358	1.72575	-0.23648
8	1998.283358	0.00385244	1.70616	-0.53367
PAM	2490.240	N/A	N/A	N/A

Table 3.3: Coefficients for WG Warm Target 4-Wire PRTs

WG PRT	R_0 [Ω]	α [°C^{-1}]	δ [°C]	β [°C]
1	1998.25965	0.00385655	1.68852	-0.01876
2	1998.174583	0.00385666	1.69379	0.07661
3	1996.419602	0.00385884	1.68682	0.03781
4	1997.806867	0.00385582	1.68417	0.19669
5	1998.913689	0.00385231	1.68385	0.18448

WG PRT	R_0 [Ω]	α [°C^{-1}]	δ [°C]	β [°C]
6	1998.242022	0.00385588	1.69594	-0.39859
7	1998.840979	0.00385434	1.68723	0.26665
PAM	2490.460	N/A	N/A	N/A

3.2 Calibration Parameters

The calibration parameters are unique to each ATMS unit and are provided in the Calibration Data Packet. The calibration parameters are needed for processing mission and housekeeping data. Table 3.4 shows the equations for converting counts to engineering units for each of these parameters. The result of each equation in Table 3.4 has a quantization error of less than 1 mK.

Table 3.4: Conversion of Calibration Parameters

Parameter	Units	Equation to Convert from Counts, C
PAM Resistance (γ_R of eqn. 3-1)	Ohms	R = 2300 + 0.006 C
4-W & 2-W PRT: R_0	Ohms	R = 1900 + 0.003 C
4-W & 2-W PRT: R'_0	Ohms	R = 1900 + 0.003 C
4-W & 2-W PRT: α	°C^{-1}	$\alpha = 0.0020 + 5x10^{-8}$ C
4-W & 2-W PRT: δ	°C	$\delta = 5.0x10^{-5}$ C
4-W PRT: β	°C	$\beta = 6.0x10^{-5}$ C – 2.0
Warm Calibration Offset	°C	T = $-7.5x10^{-6}$ C
Cold Calibration Offset	°C	T = $3.0x10^{-5}$ C
Quadratic Coefficient	K^{-1}	$A_2 = 3.05x10^{-9}$ C - 0.0001
Alignment	Degrees	$\theta = 2.0x10^{-5}$ C – 0.655
2-W PRT: A_1	°C /Ohm	$A_1 = 3.0x10^{-6}$ C
Rc	Ohms	R = 0.0003 C
MUXRESTi	Ohms	R = 1900 + 0.003C

3.3 Receiver Shelf and Other 2-Wire PRTs

The instrument has 4 receiver shelf 2-wire PRTs – one for each of the 4 receiver shelves (the K/Ka-band receiver shelf, W-band receiver shelf, G-band receiver shelf, and V-band receiver shelf).

Processing of the receiver shelf 2-wire PRTs is identical to the 4-wire PRT processing, using the WG 4-wire parameters for γ_R, γ_0, and γ_1; except that β is assumed to be 0 and is not transmitted as part of the Calibration Packet for those sensors. R_0, α and δ are provided in words #140-155 of the Calibration Packet. The cable resistance, R_C, is also provided, for use in the counts-to-resistance conversion (equation 3-1).

Table 3.5 lists the coefficients for the receiver shelf PRTs.

Table 3.5: Coefficients for Receiver Shelf 2-Wire PRT's

Mnemonic	R_0(Ω)	α (°C^{-1})	δ (°C)	R_C(Ω)
KKA_SHELF_PRT	1995.340480	0.00384400	2.16964	0.768
V_SHELF_PRT	1995.535350	0.00387361	0.85582	0.849

Mnemonic	R_0(Ω)	α (°C^{-1})	δ (°C)	R_C(Ω)
W_SHELF_PRT	1998.606130	0.00385020	1.66407	0.849
G_SHELF_PRT	1997.378090	0.00384990	1.65872	0.647

.

The 27 other 2-wire PRTs, including the mnemonic for the Scan Drive Mechanism (SDM) temperature and SD Power Supply (PS), are used purely as health and status indicators and do not require the same precision as the 4-wire PRTs and receiver shelf PRTs. These temperatures, therefore, are processed according to the following linear equation, except for the scan drive PRTs (which are processed without using any parameters contained in the Calibration packet):

$$T = A_1 (R - R_0) = A_1 (R' - R'_0)$$ Equation 3-4

$$R' = R + Rc = \gamma_R (C - \gamma_0) / (\gamma_1 - \gamma_0)$$ Equation 3-5

$$R'_0 = R_0 + R_C$$ Equation 3-6

Where T is the temperature, in degrees Celsius, R_0' and A_1 are parameters transmitted in the Calibration Data Packet, words 156-211

The parameter A_1 is related to the Callendar-Van Dusen parameters by the following equation:

$$A_1 = \frac{1}{\alpha(1+\delta/100)R_0}$$ Equation 3-7

Table 3.6 lists the coefficients of the other 2-wire PRTs.

Table 3.6: Coefficients for Other 2-Wire PRTs

Mnemonic	R_0 (Ω)	α (°C^{-1})	δ (°C)	Rc (Ω)	R_0' (Ω)	A_1 (°C/ Ω)
K_RFE_PRT	1995.380770	0.00387310	0.96459	0.648	1996.028770	0.12816
KA_RFE_PRT	1997.13982	0.0039152	1.59588	0.648	1997.78782	0.125881376
V_RFE_PRT	1994.09404	0.0038524	1.94229	0.892	1994.98604	0.127693445
V_PRI_PLO_PRT	1996.23356	0.00385584	1.6231	0.851	1997.08456	0.127843074
V_RED_PLO_PRT	1997.07342	0.003853	1.63079	0.77	1997.84342	0.127873826
V2_IF_PRT	1996.84174	0.0038405	1.71185	0.851	1997.69274	0.128202658
W_RFE_PRT	1994.69985	0.0038474	1.81542	0.851	1995.55085	0.127979835
SAW_FILT_PRT	1995.76364	0.00385775	1.61843	0.932	1996.69564	0.127815738
W_IF_PRT	1993.72998	0.0038568	1.75007	0.81	1994.53998	0.127812057
WG1_PRI_82LO_PRT	1997.11018	0.00385241	1.65957	0.81	1997.92018	0.127854849
WG1_RED_82LO_PRT	1994.73714	0.00385553	1.66289	0.689	1995.42614	0.127899188
G2_PRI_91LO_PRT	1996.78462	0.003851	1.71385	0.77	1997.55462	0.127854249
G2_RED_91LO_PRT	1994.3053	0.0038422	2.35085	0.689	1994.9943	0.127507854
G1_IF_PRT	1997.15885	0.003853	1.66	0.851	1998.00985	0.127831615
G2_IF_PRT	1993.81921	0.0038554	1.63504	0.851	1994.67021	0.12799745
RCVPS_A_PRT	1997.66932	0.00384485	2.59322	0.6	1998.26932	0.126904884
RCVPS_B_PRT	1994.49796	0.00386599	1.79321	0.6	1995.09796	0.127405116

Mnemonic	R_0 (Ω)	α (°C^{-1})	δ (°C)	Rc (Ω)	R_0' (Ω)	A_1 (°C/ Ω)
OCXO_PRI_PRT	1999.7692	0.00384539	1.72952	0.891	2000.6602	0.127829985
OCXO_RED_PRT	1994.07509	0.00385824	1.89717	0.972	1995.04709	0.127557832
DSPA_1553_PRT	1999.549889	0.00385263	1.75473	0.1	1999.649889	0.127572142
DSPB_1553_PRT	1999.459911	0.00385304	1.66702	0.1	1999.559911	0.127674359
SPA_PS_A_PRT	1997.24161	0.00384262	1.60635	0.1	1997.34161	0.12823929
SPA_PS_B_PRT	1994.3353	0.00384695	1.52493	0.1	1994.4353	0.128384497
DSPA_PROC_PRT	1999.362215	0.003851	1.73898	0.1	1999.462215	0.127657878
DSPB_PROC_PRT	1999.33344	0.00386319	1.15714	0.1	1999.43344	0.127988857

3.4 Other Engineering Data

For engineering data such as voltages (except for the Scan Drive Subsystem), the measured parameter is defined by the linear equation:

$$[\text{parameter}] = m\,C + b \qquad \text{Equation 3-8}$$

where

C is the data count reported for the parameter,
m is the product of the A/D conversion and the scale factor
b is the offset.

Table 3.7 indicates the scale and offset values for these parameters included in the LEO&A, Engineering, and Housekeeping data packets.

Table 3.7: Voltage Scale and Offset Parameters

Mnemonic	Word #	Units	m	b
SPA_P5V_VMON	2	Volts	8.5832E-05	0.00
SPA_P15V_VMON	3	Volts	2.7466E-04	0.00
SPA_N15V_VMON	4	Volts	-2.7466E-04	0.00
RCV_P6V_RF_VMON	5	Volts	1.0717E-04	0.00
RCV_P12V_RF_VMON	6	Volts	2.12505E-04	0.00
RCV_P15V_RF_VMON	7	Volts	2.5628E-04	0.70
RCV_N15V_RF_VMON	8	Volts	-2.5628E-04	-0.70
RCV_P15V_ANA_VMON	9	Volts	2.6560E-04	0.00
RCV_N15V_ANA_VMON	10	Volts	-2.6560E-04	0.00
V_PLO_A_LOCK_VMON	42	Volts	2.0399E-04	0.00
V_PLO_B_LOCK_VMON	43	Volts	2.0399E-04	0.00
VD_REF_MOD1	48	Volts	6.8666E-05	0.00
VD_REF_MOD2	49	Volts	6.8666E-05	0.00
VD_REF_MOD3	50	Volts	6.8666E-05	0.00
VD_REF_MOD4	51	Volts	6.8666E-05	0.00
VD_GND_MOD1	52	Volts	6.8666E-05	0.00
VD_GND_MOD2	53	Volts	6.8666E-05	0.00
VD_GND_MOD3	54	Volts	6.8666E-05	0.00
VD_GND_MOD4	55	Volts	6.8666E-05	0.00

Telemetry processing equations for the Scan Drive Subsystem are given in Table 3.8.

Table 3.8: Data Conversions for Scan Drive Engineering Telemetry

Telemetry Parameter	Word #	Measurement Variable	Nominal Value	Conversion Algorithms
SDM Temperature	40	Count	518 Counts (at 15°C)	$T_{DegC} = \frac{1{,}000{,}000 \times (Count - 399.3371)}{8{,}905{,}947 - (1{,}907.3 \times Count)}$
SD PS Temperature	41	Count	518 Counts (at 15°C)	$T_{DegC} = \frac{1{,}000{,}000 \times (Count - 399.3371)}{8{,}905{,}947 - (1{,}907.3 \times Count)}$
+5V	56	Count1	1002 Counts	$V_5 = \frac{5008}{Count1}$
+12V	57*	Count3	804 Counts	$V_{12P} = \left[\frac{(4.284 \times Count3) - (45.08657 \times Count2)}{Count1}\right] + 43.30089$
-12V	58*	Count2	772 Counts	$V_{12N} = \left[\frac{63.096 \times Count2}{Count1}\right] - 60.6212$
Main Motor Current	59*	Count	0.0 Amps	$MainMotorCur = (0.021777 \times Count) - 0.3888$
Comp Motor Current	60*	Count	0.1 Amps	$CompMotorCur = (0.021777 \times Count) - 0.3888$
Resolver Excitation Voltage (V_{RMS})	61*	Count	7.2 Volts	$ResExV = 0.008817 \times Count$
Main Motor Velocity	62*	Count	60 degr/sec	$MainVel = 0.0625 \times Count$
Comp Motor Velocity	63*	Count	- 100 degr/sec	$CompVel = 0.0625 \times Count$
Main Loop Position Error	64*	Count	0.01 degrees	$Perr = 0.005493164 \times Count$
Main Loop Integrated Error	65*	Count	3.6 degrees	$PerrInteg = 0.005493164 \times Count$
Main Loop Velocity Error	66*	Count	2.0 degr/sec	$VelErr = 0.0625 \times Count$
Comp Loop Velocity Error	67*	Count	-5.0 degr/sec	$CompVelErr = 0.0625 \times Count$
Requested Main Motor Voltage	68*	Count	0.3 Volts	$MainMV = 0.0005493164 \times Count$
Requested Comp Motor Voltage	69*	Count	-0.5 Volts	$CompMV = 0.0005493164 \times Count$
Feed Forward Voltage	70*	Count	28 Volts	$FFV = \frac{458{,}752}{Count}$

Telemetry Parameter	Word #	Measurement Variable	Nominal Value	Conversion Algorithms
Comp Motor Position	71*	Count	70 degrees	$CompMP = 0.005493164 \times Count$

* Words #59 – 71 are signed; The Scan Drive -12V monitor is dependent on the result of the +5V monitor; The Scan Drive +12V monitor is dependent on the results of the +5V and -12V monitors.

3.5 Limits for Passive Analog Temperature Telemetry and Housekeeping Data

The operating limits of the instrument are driven by the ATMS Cold plate temperature. In the sections 3.5.1 – 3.5.2 below, the advance warning temperatures of potential damage risk are provided.

3.5.1 Limits for Passive Analog Temperature Telemetry

The passive analog temperature telemetry channels are provided on spacecraft interface primary and redundant connectors to sample instrument temperatures. These temperatures are accessible whether the instrument is powered "Off" or "On". The limits for passive analog temperature telemetry are shown in Table 3.9. The yellow limits are an advance warning of impending damage risk.

Table 3.9: Passive Analog Temperature Telemetry Operational Warning Limits in Celsius

Mnemonic	Description	Operational Limits	
		Yellow Limit (low)	Yellow Limit (high)
SDM_TEMP	Temperature of Scan Drive Mechanism (Degrees C)	-22	46
CAL_TARGET_LOC_TEMP	Temperature of Bench, near Hot Calibration Targets (Degrees C)	-23	60
KKAV_SHELF_TEMP	Temperature on the V-Band Receiver Shelf (Degrees C)	-10	50
WG_SHELF_TEMP	Temperature on the G-Band Receiver Shelf (Degrees C)	-10	50
INSTR_BASEPLATE_TEMP	Temperature of the Instrument Baseplate (Degrees C)	-22	35

3.5.2 Limits for Housekeeping Data

Housekeeping telemetry is made available to the spacecraft via the MIL-STD-1553 bus as engineering data in the housekeeping (APID 0x206), LEO&A (APID 0x201), and Engineering H&S (APID 0x213) packets. This data is used to assess the health and status of the instrument. The limits for housekeeping telemetry are shown in Table 3.10. These yellow limits are an advance warning of impending damage risk.

Table 3.10: Housekeeping Telemetry Advanced Warning Operational Limits

Housekeeping Telemetry Advanced Warning Operational Limits				
Word #	**Mnemonic**	**Description**	**Yellow Limit (low)**	**Yellow Limit (high)**
2	SPA_P5V_VMON	Voltage Monitor [V]	4.7	5.4
3	SPA_P15V_VMON	Voltage Monitor [V]	14.25	15.75
4	SPA_N15V_VMON	Voltage Monitor [V]	-15.75	-14.25
5	RCV_P6V_RF_VMON	Voltage Monitor [V]	5.75	6.50
6	RCV_P12V_RF_VMON	Voltage Monitor [V]	11.25	12.75
7	RCV_P15V_RF_VMON	Voltage Monitor [V]	14.25	15.75
8	RCV_N15V_RF_VMON	Voltage Monitor [V]	-15.75	-14.25
9	RCV_P15V_ANA_VMON	Voltage Monitor [V]	14.25	15.75
10	RCV_N15V_ANA_VMON	Voltage Monitor [V]	-15.75	-14.25
11	K_RFE_PRT	Temp Monitor (2-wire PRT) [°C]	-15	55
12	KA_RFE_PRT	Temp Monitor (2-wire PRT) [°C]	-15	55
13	V_RFE_PRT	Temp Monitor (2-wire PRT) [°C]	-15	55
14	V_PRI_PLO_PRT	Temp Monitor (2-wire PRT) [°C]	-15	55
15	V_RED_PLO_PRT	Temp Monitor (2-wire PRT) [°C]	-15	55
16	V2_IF_PRT	Temp Monitor (2-wire PRT) [°C]	-15	55
17	W_RFE_PRT	Temp Monitor (2-wire PRT) [°C]	-15	55
18	SAW_FILT_PRT	Temp Monitor (2-wire PRT) [°C]	-15	55
19	W_IF_PRT	Temp Monitor (2-wire PRT) [°C]	-15	55
20	WG1_PRI_82LO_PRT	Temp Monitor (2-wire PRT) [°C]	-15	55
21	WG1_RED_82LO_PRT	Temp Monitor (2-wire PRT) [°C]	-15	55
22	G2_PRI_91LO_PRT	Temp Monitor (2-wire PRT) [°C]	-15	55
23	G2_RED_91LO_PRT	Temp Monitor (2-wire PRT) [°C]	-15	55
24	G1_IF_PRT	Temp Monitor (2-wire PRT) [°C]	-15	55

Housekeeping Telemetry Advanced Warning Operational Limits				
Word #	**Mnemonic**	**Description**	**Yellow Limit (low)**	**Yellow Limit (high)**
25	G2_IF_PRT	Temp Monitor (2-wire PRT) [°C]	-15	55
26	W_SHELF_PRT	Temp Monitor (2-wire PRT) [°C]	-15	50
27	KKA_SHELF_PRT	Temp Monitor (2-wire PRT) [°C]	-15	50
28	G_SHELF_PRT	Temp Monitor (2-wire PRT) [°C]	-15	50
29	V_SHELF_PRT	Temp Monitor (2-wire PRT) [°C]	-15	50
30	RCVPS_A_PRT	Temp Monitor (2-wire PRT) [°C]	-20	55
31	RCVPS_B_PRT	Temp Monitor (2-wire PRT) [°C]	-20	55
32	OCXO_PRI_PRT	Temp Monitor (2-wire PRT) [°C]	-20	40
33	OCXO_RED_PRT	Temp Monitor (2-wire PRT) [°C]	-20	40
34	DSPA_1553_PRT	Temp Monitor (2-wire PRT) [°C]	-15	55
35	DSPB_1553_PRT	Temp Monitor (2-wire PRT) [°C]	-15	55
36	SPA_PS_A_PRT	Temp Monitor (2-wire PRT) [°C]	-20	55
37	SPA_PS_B_PRT	Temp Monitor (2-wire PRT) [°C]	-20	55
38	DSPA_PROC_PRT	Temp Monitor (2-wire PRT) [°C]	-15	55
39	DSPB_PROC_PRT	Temp Monitor (2-wire PRT) [°C]	-15	55
40	SD_MECH_TEMP*	Temp Monitor (2-wire PRT) [°C]	-15	46
41	SD_PS_PRT*	Temp Monitor (2-wire PRT) [°C]	-15	55
42	V_PLO_A_LOCK_VMON	Voltage Monitor [V]	-999	0.35
43	V_PLO_B_LOCK_VMON	Voltage Monitor [V]	-999	0.35
44	HK_2WREST1_A or _B	HK 2 Wire Reference 1	45000	55000
45	HK_2WREST2_A or _B	HK 2 Wire Reference 2	45000	55000
46	4W_GND_A or _B	4 Wire GND	0	2000
47	2W_GND_A or _B	2 Wire GND	0	2000
48	VD_REF_MOD1	Voltage Reference [V]	1.8	2.7

Housekeeping Telemetry Advanced Warning Operational Limits				
Word #	**Mnemonic**	**Description**	**Yellow Limit (low)**	**Yellow Limit (high)**
49	VD_REF_MOD2	Voltage Reference [V]	1.8	2.7
50	VD_REF_MOD3	Voltage Reference [V]	1.8	2.7
51	VD_REF_MOD4	Voltage Reference [V]	1.8	2.7
52	VD_GND_MOD1	Gnd Reference [V]	-0.5	0.5
53	VD_GND_MOD2	Gnd Reference [V]	-0.5	0.5
54	VD_GND_MOD3	Gnd Reference [V]	-0.5	0.5
55	VD_GND_MOD4	Gnd Reference [V]	-0.5	0.5
56	SD_P5V_VMON	Scan Drive Monitor (Voltage) [V]	4.7	5.4
57	SD_P12V_VMON	Scan Drive Monitor (Voltage) [V]	10.3	13.7
58	SD_N12V_VMON	Scan Drive Monitor (Voltage) [V]	-13.7	-10.3
59	MAIN_MOTOR_CUR**	Scan Drive Monitor (Current) [A]	-5.5	5.5
60	COMP_MOTOR_CUR**	Scan Drive Monitor (Current) [A]	-6.06	6.06
61	RESOLVER_VMON	Scan Drive Monitor (Voltage) [V]	6.3	7.7
62	SD_MAIN_MOTOR_VEL	Scan Drive Monitor (Velocity) [°/s]	-800	800
63	SD_COMP_MOTOR_VEL	Scan Drive Monitor (Velocity) [°/s]	-800	800
64	SD_MAIN_LOOP_ERROR	Scan Drive Main Loop Position Error [°]	-0.04	0.04
65	SD_MAIN_LOOP_INT_ERROR	Scan Drive Main Loop Internal Error [°]	-0.05	25
66	SD_MAIN_LOOP_VEL_ERROR	Scan Drive Main Loop Velocity Error [°/s]	-100	200
67	SD_COMP_LOOP_ERROR	Scan Drive Comp. Loop Velocity Error [°/s]	-300	150
68	SD_MAIN_MOTOR_REQ_VOLTAGE	SD Requested Main Motor Voltage [V]	-3	3
69	SD_COMP_MOTOR_REQ_VOLTAGE	SD Requested Comp. Motor Voltage [V]	-5	5
70	SD_FEED_FORWARD_VOLTAGE	Scan Drive Monitor (Voltage) [V]	20	36

Note: Nominal low/high temperature limits are based on -10° C/+20° C instrument base plate temperature;
* B-side SDE produces invalid telemetry for these temperature sensors,
** B-side telemetry is ignored due to negative values.

The following housekeeping telemetry assignments in Table 3.11 are checked against limits in ATMS Flight Software:

Table 3.11: Flight Software Limits for Motor Currents

Mnemonic	Word #	Description	Low Limit	High Limit
MAIN_MOTOR_CUR	59	Scan Drive Current Monitors (Amperes)	-0.3888	15.008
COMP_MOTOR_CUR	60	Scan Drive Current Monitors (Amperes)	-0.3888	15.008

If the main motor or compensator motor current exceeds the low or high limits for 2 consecutive housekeeping packets, the ATMS will automatically enter Safehold mode.

4. REFLECTOR POSITION DATA

The scan angle value for each science data sample is provided in data word number 1 of the Science Data Packet, APID 210_{16} (APID 528_{10}) for operational data and APID 218_{16} (APID 536_{10}) for diagnostic data. The reflector position is reported by a 16-bit word, so resolver counts range from 0, nominally at nadir, to 65,535. The full 16-bit range corresponds to 360 degrees, so the scale factor is 5.493164×10^{-3} degrees per count. Figure 4-1 depicts the relative beam position geometry for a scan.

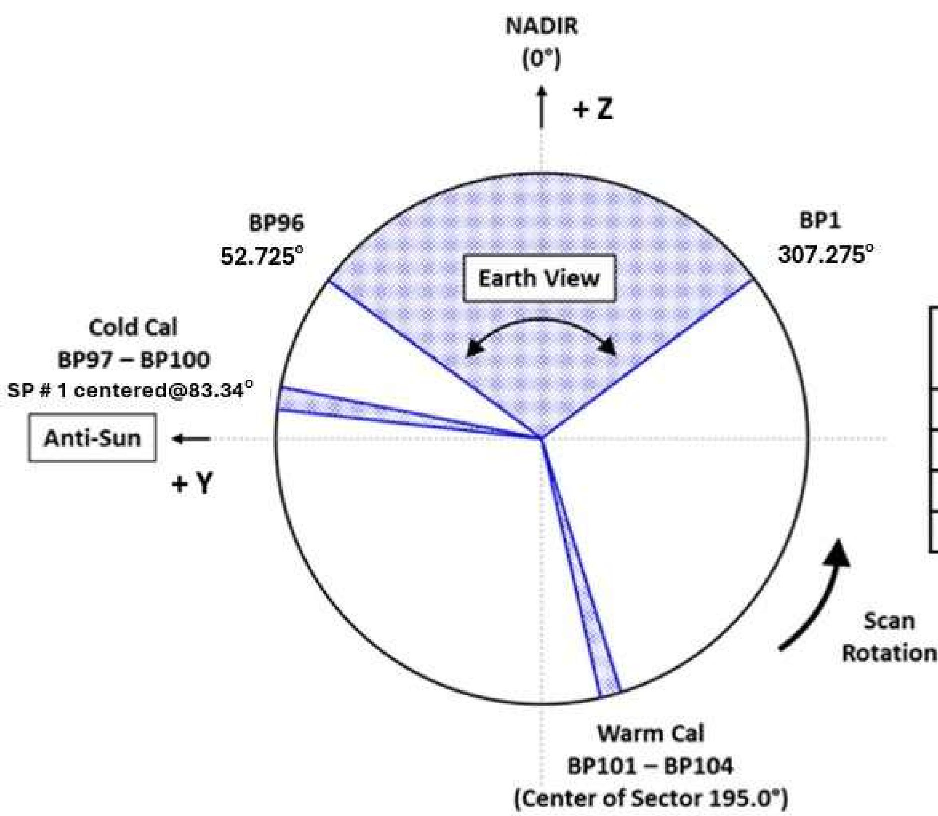

Profile No. SP #	Cold Cal Angle
1	83.34°
2	81.67°
3	80.00°
4	76.67°

Figure 4-1: Beam Position and Scan Geometry

The ATMS Flight Software (FSW) supports 4 independent scan profiles as shown in Figure 4-1. During ATMS power on, the instrument specific scan tables are loaded from the SPA DSP CCA EEPROM to a specific portion of FSW Data RAM. A single scan profile table is then selected and loaded from FSW Data RAM into the Scan Drive Electronics (SDE) RAM by using the "Scan Profile" (SP) command. While the reflector position (resolver angle) is reported in Science Data as a 16-bit word, the commanded scan angle data is stored in SDE RAM as 24-bit words. To properly fill the SDE RAM, each angle of the scan profile table is stored in SPA EEPROM as two 16-bit words. Each scan consists of 592 positions. These positions define the scan positions for a time interval of ~ 4.5 msec.
The actual interval is:

8/3 seconds/scan / 592 positions/scan ≈ 4.504504 msec/position

Therefore, the area of SDE RAM utilized for the scan table consists of 592 24-bit words while the area of SPA EEPROM utilized for each scan profile consists of 1184, 16-bit words following Big-Endian convention where the byte order has the most significant byte of a multibyte value in the lowest storage address.

For each scan position in the SPA EEPROM, only the upper 8 bits of the MSW are used while the LSW contains the lower 16-bits of the scan angle. The MSW is defined Table 4.1. The 18-bit scan angle as stored in the SDE may be created by the notation in Figure 4-2 following Big-Endian convention.

Table 4.1: SPA EEPROM Scan Position MSW Definition

Bit	Description
0 – 7	Unused
8 – 9	Upper 2 bits of the scan angle
10	Transmit Reflector Position Flag
11	Beam Boundary Flag
12 – 15	Unused

Word	MSW		LSW															
Bit	9	8	15	14	13	12	11	10	9	8	7	6	5	4	3	2	1	0

Figure 4-2: SPA EEPROM 18-bit Scan Position Notation

The resolver offset between the actual antenna beam position to the reported Scan Drive Mechanism (SDM) resolver position is defined by the following equation.

$$Offset = SDM\ Resolver\ Angle - RF\ Beam\ Angle \qquad \text{Equation 4-1}$$

For QS ATMS S/N 301, there is no resolver offset (i.e., +0.00°, corresponding to zero counts). The conversion from 16-bit reflector position counts, in Science Data packets, C, to angular degrees is:

$$\theta = \frac{360}{2^{16}} \times mod(C, 2^{16}) \qquad \text{Equation 4-2}$$

Similar to the resolver telemetry, the point and stare command takes a 16-bit argument, and the motor is maintained at the corresponding 16-bit resolver position. To obtain the point and stare 16-bit argument for a desired angle the following equation should be used:

$$C = round\left(\frac{2^{16}}{360°} \times mod(\theta, 360°)\right) \qquad \text{Equation 4-3}$$

To perform the 18-bit conversion for scan table commanded reflector position contained in the scan profile table in the SDE RAM and SPA EEPROM the following equation shall be used:

$$\theta = \frac{360}{2^{18}} \times mod(C, 2^{18}) \qquad \text{Equation 4-4}$$

Table 4.2: QS ATMS Spaceview and Warm Load Reading Resolver Counts for Scan Profile 1

Beam Position	Expected Resolver Counts
97	14868
98	15070
99	15272
100	15475
101	35196
102	35398
103	35603
104	35802

The timing of the beam position samples relative to the 8-second synchronization pulse is illustrated in Figure 4-3. The delay between the synchronization pulse and the start of the beam position 1 sample is set by a programmable (upload-able) offset. For S/N 301, the default programmable scan offset is set to 559.917 msec. With this offset there is 2.118 seconds from receipt of the spacecraft (S/C) scan synchronization pulse to the start of beam position one data collection.

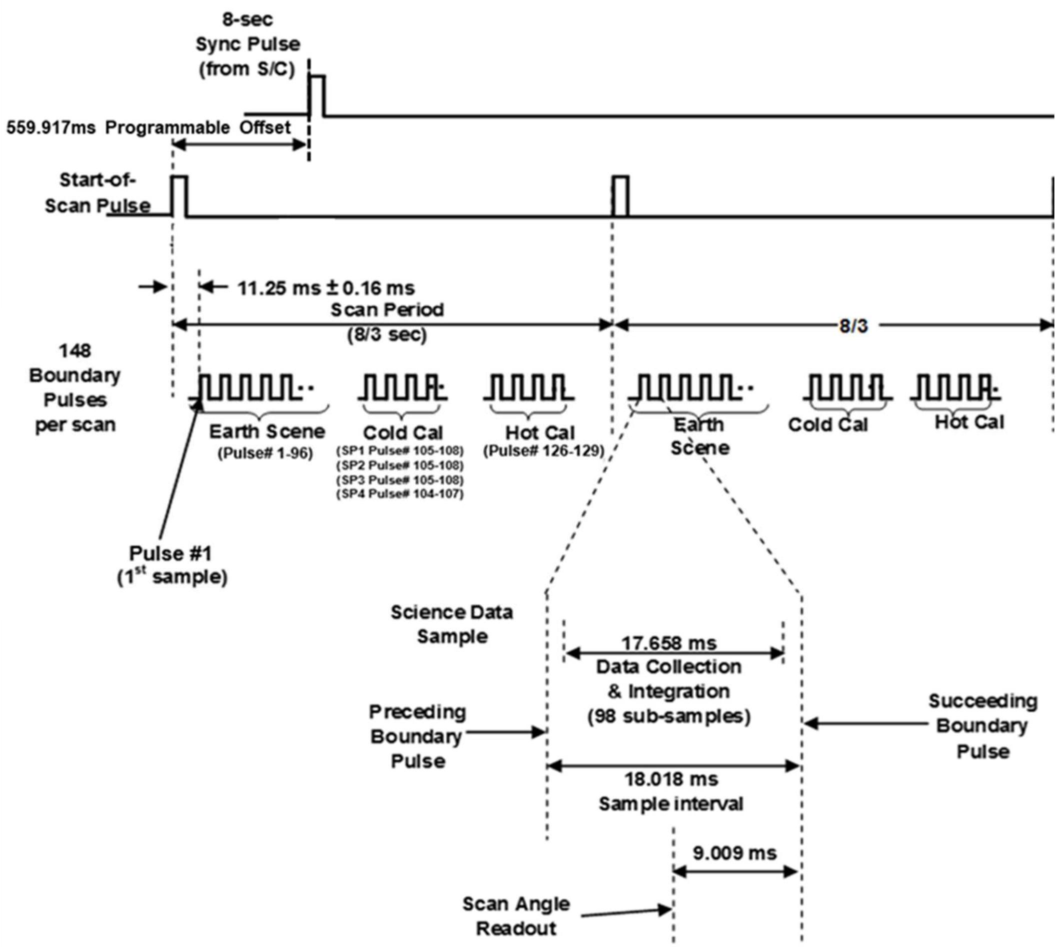

Scan angle readout and center of integrated data sample both occur at the center of the sample interval: 9.009 ms prior to the succeeding boundary pulse.

Time tag for each science data packet corresponds to the succeeding boundary pulse.

First Earth-View boundary pulse (beginning of first sample) of every third scan precedes the 8-sec scan sync pulse by a programmable offset. If offset is zero, the beginning of first sample coincides with scan sync pulse.

Figure 4-3: ATMS Beam Position with Respect to 8-Second Synchronization Pulse (Not to scale)

5. ANTENNA PATTERN DATA

For the on-orbit calibration of the ATMS instrument, antenna pattern data is utilized in both radiance calibration and brightness temperature calibration, based on the modified Rayleigh-Jeans approximation.

- Section 5.1 covers the processing of antenna data and its performance analysis.
- Section 5.2 introduces antenna beam pointing offsets and instrument mounting errors, which are essential for geolocation processing.

- Section 5.3 presents the emissivity datasets of the antenna's flat reflector, derived from cold space scan observations collected during the post-launch pitch-maneuver test. These emissivity data are used for reflector emission correction in radiance calibration.
- Section 5.4 details the antenna pattern correction coefficients, which are used to convert antenna temperature data record products (TDR) into sensor data record (SDR) within the radiance calibration algorithm. Additionally, these coefficients can be applied to the brightness temperature calibration algorithm at the user's discretion.

5.1 Antenna Performance Data

For QS ATMS, antenna patterns measurements have been made for antenna performance evaluation and there is no separate measurement for beam pointing offset assessment. For antenna performance evaluation, the antenna pattern was measured at four different scan positions (Earth view scan position 1, 48, 96, and cold space view) for 15 frequencies from 23 to 183 GHz, with each measurement for channels 1 to 9, one single measurement for channels 10 to 15, each measurement for channels 16 and 17, each measurement for low, mid and high 183 GHz channels, i.e., 176.31, 183.31, and 190.31 GHz, respectively. The antenna pattern data was collected at two different azimuth directions of 0, 90 for elevation angle from -179 to 179 degrees. Interpolations are made to derive antenna pattern for azimuth angle of 45 and 135 degrees. For channels 1, 2 and 16, the data was measured with 0.1 degrees resolution, and 0.05 degrees for other channels. To compute the antenna main beam performance and the side lobe contamination, the original measurement profiles were interpolated to two-dimensional space for azimuth angles from -179 to 180 with 1 deg resolution, and elevation angles from -179 to 180, with 0.01 deg resolution. The two-dimensional antenna pattern data are generated for all 96 Earth scan FOVs and the 4 space view FOVs, see Figure 5-1 and Figure 5-2.

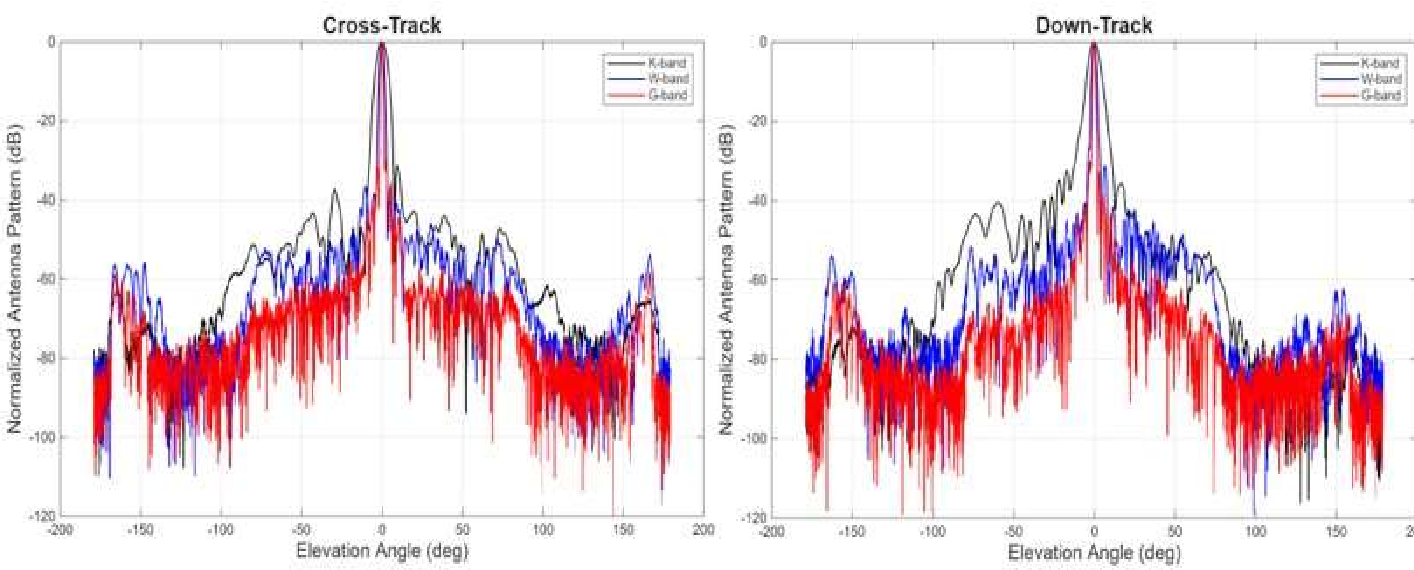

Figure 5-1: Antenna pattern measurements at the nadir scan position for K-, W- and G- band. Left is for cross-track (0-degree azimuth angle) and right is for down-track (90 degree azimuth angle)

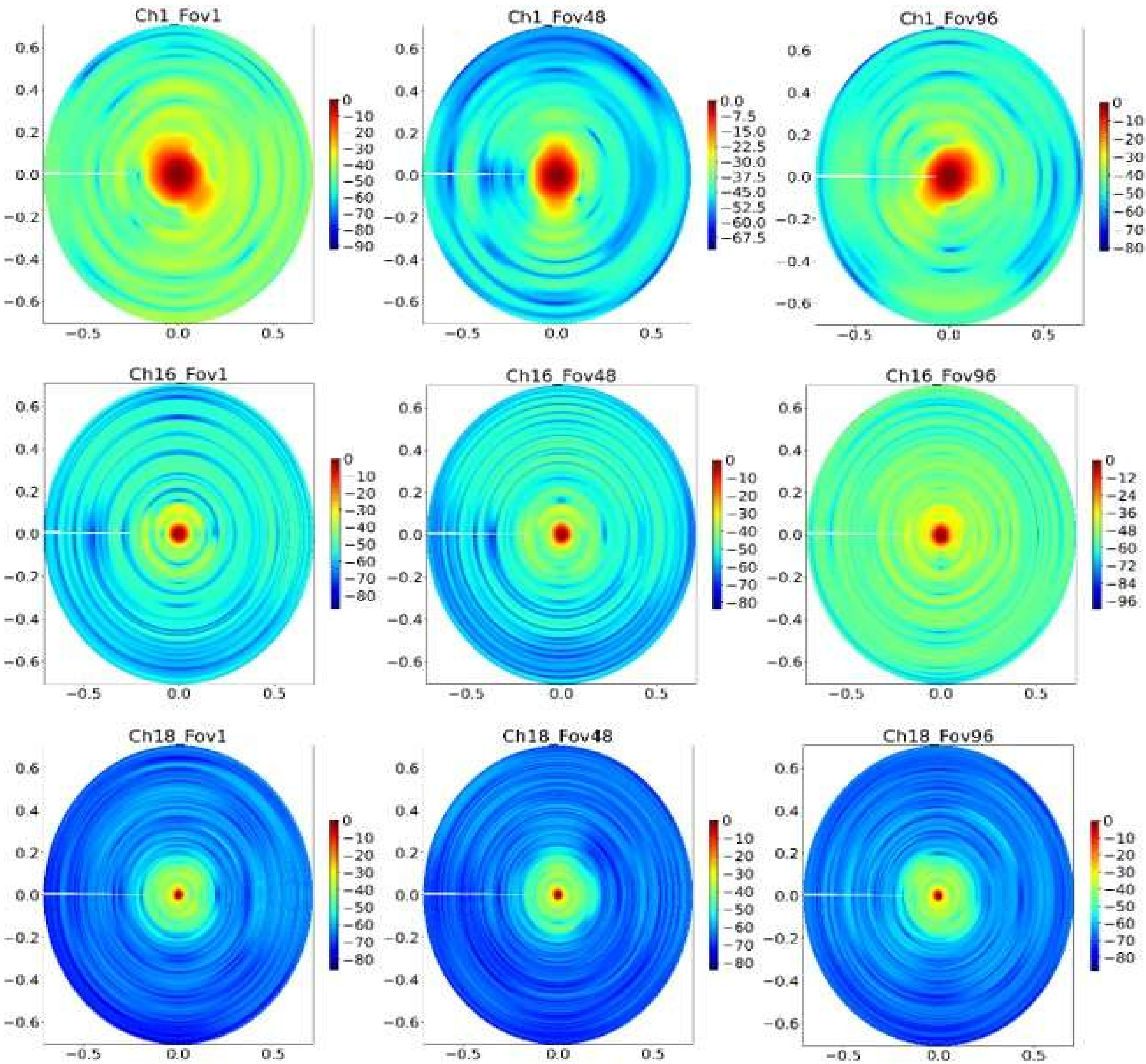

Figure 5-2: Reprocessed 2-D antenna pattern data at scan positions 1, 48 and 96 for channels 1, 16 and 18.
X and Y axis are the projected positions in Cartesian coordinates. Color bar is the normalized antenna pattern in dB.

Table 5.1 below lists the calculated antenna 3 dB beam width (in deg.) and main beam efficiency (unitless) at the scan positions of FOV 1, 48 and 96. Note main beam efficiency is integrated out to 2.5 times the 3 dB beam width.

Table 5.1: The calculated antenna parameters for the nadir scan position of FOV 1, 48, 96

Channel #	BeamWidth (deg, FOV01)	Beam Width (deg, FOV48)	Beam Width (deg, FOV96)	Main beam efficiency (FOV01)	Main beam efficiency (FOV48)	Main beam efficiency (FOV96)
1	5.20	5.17	5.25	0.9560	0.9575	0.9635
2	5.37	5.35	5.37	0.9802	0.9667	0.9767
3	2.17	2.12	2.12	0.9749	0.9618	0.9700
4	2.12	2.20	2.17	0.9719	0.9678	0.9741
5	2.15	2.12	2.12	0.9736	0.9685	0.9716
6	2.12	2.15	2.15	0.9750	0.9704	0.9720
7	2.12	2.12	2.10	0.9800	0.9723	0.9786
8	2.10	2.12	2.10	0.9798	0.9744	0.9795
9	2.10	2.10	2.15	0.9795	0.9730	0.9797
10	2.07	2.10	2.12	0.9752	0.9734	0.9817
11	2.07	2.10	2.12	0.9752	0.9734	0.9817
12	2.07	2.10	2.12	0.9752	0.9734	0.9817
13	2.07	2.10	2.12	0.9752	0.9734	0.9817
14	2.07	2.10	2.12	0.9752	0.9734	0.9817
15	2.07	2.10	2.12	0.9752	0.9734	0.9817
16	2.02	2.02	2.02	0.9514	0.9514	0.9514
17	1.05	1.05	1.05	0.9550	0.9550	0.9550
18	1.10	1.11	1.12	0.9550	0.9555	0.9580
19	1.10	1.11	1.12	0.9550	0.9555	0.9580
20	1.10	1.10	1.11	0.9599	0.9593	0.9558
21	1.10	1.10	1.11	0.9599	0.9593	0.9558
22	1.10	1.10	1.11	0.9599	0.9593	0.9558

5.2 Antenna Beam Pointing Offset Data

Antenna beam pointing error includes the error from the antenna beam misalignment and the error from the instrument mounting. For QS ATMS, the beam misalignment measurements are missing. For evaluation of the antenna beam pointing offset, only the instrument mounting bias is derived by using the post-satellite TVAC instrument mounting matrix measurements, the Euler angles for beam pointing errors are then calculated in predefined satellite coordinates. The Euler angles including the instrument mounting bias for QS ATMS are listed in Table 5.2. For on-orbit geolocation processing, the beam pointing offset Euler angles at each scan position will be interpolated from the scan positions 1, 48 and 96. A 3x3 rotation matrix can then be constructed following equation 5-1 to transfer the beam vector from the antenna system to the satellite coordinate system.

$$Rot_{\hat{b}p_{atms}->\vec{b}p_{atms}}(x = roll, y = pitch, z = yaw) = \begin{pmatrix} \cos Y \cos Z - sinXsinYsinZ & -sinZcosX & cosZsinY + sinXcosYsinZ \\ sinZcosY + sinXsinYcosZ & \cos X \cos Z & sinZsinY - sinXcosZcosY \\ -cosXsinY & \sin X & \cos X \cos Y \end{pmatrix}$$

Equation 5-1

Table 5.2: The Euler angles for QS ATMS antenna beam pointing offset in Satellite Coordinates in degrees, at scan positions 1, 48 and 96 (To be updated by using post-sat TVAC data)

Band	BP1_Roll	BP1_Pitch	BP1_Yaw	BP48_Roll	BP48_Pitch	BP48_Yaw	BP96_Roll	BP96_Pitch	BP96_Yaw
K	-0.087	0.018	-0.906	-0.157	0.011	-0.908	-0.150	-0.015	-0.893
KA	-0.067	0.091	-0.870	-0.111	0.043	-0.908	-0.129	-0.021	-0.890
V	-0.026	0.074	-0.879	-0.103	-0.013	-0.908	-0.145	-0.069	-0.866
W	-0.111	-0.010	-0.920	-0.103	0.030	-0.908	-0.094	0.053	-0.927
G	-0.097	-0.027	-0.929	-0.082	0.025	-0.908	-0.090	0.074	-0.937

5.3 Antenna Flat Reflector Emissivity (To be updated by using Post-Launch Pitch Maneuver Test data)

The antenna emissivity, ϵ_h, at 45° angle with respect to the scattering plane can be solved with the following equation [1]:

$$\epsilon_h = \frac{\delta \cdot (R_w - R_c)}{\delta \cdot [(R_w - R_{rfl}) \cdot sin^2\theta_w - (R_c - R_{rfl}) \cdot sin^2\theta_c] - (R_c - R_{rfl}) \cdot (sin^2\theta_s - sin^2\theta_c)}. \quad \text{Equation 5-2}$$

In equation above, R_w, R_c, and R_{rfl} represent the warm load, cold space view and antenna reflector radiance, respectively. Meanwhile, the parameters θ_w, θ_c, and θ_s respectively represent the scan angle associated with the warm load, space view, and scene. Finally, $\delta = (C_s - C_c)/(C_w - C_c)$ is the normalized scene counts. The channel-dependent flat reflector emissivities of QS ATMS are derived from on-orbit pitch maneuver observations by using equation 5-2 and are listed in Table 5.3. Note $\epsilon_v = 2 * \epsilon_h$. The ϵ_v can be derived in a similar way with ϵ_h.

Table 5.3: QS ATMS Reflector Emissivity (Data from SNPP, TBD for QS)

Channel	QS ATMS Reflector Emissivity ϵ_h
1	0.00347
2	0.00237
3	0.00222
4	0.00222
5	0.00222
6	0.00222
7	0.00231

Channel	QS ATMS Reflector Emissivity ϵ_h
8	0.00231
9	0.00231
10	0.00249
11	0.00249
12	0.00249
13	0.00249
14	0.00249
15	0.00249
16	0.00383
17	0.00373
18	0.00392
19	0.00392
20	0.00392
21	0.00392
22	0.00392

For on-orbit calibration, the cold space view and warm load radiance are corrected for reflector emission by using the equation below:

For Q_v channels

$$\Delta R_{x,reflEmis} = \epsilon_h \cdot \left(R_{rfl} - R_x\right) + \left(R_{rfl} - R_x\right) \cdot (\epsilon_v - \epsilon_h) \cdot sin^2\theta \,. \qquad \text{Equation 5-3}$$

For Q_h channels

$$\Delta R_{x,reflEmis} = \epsilon_h \cdot \left(R_{rfl} - R_x\right) + \left(R_{rfl} - R_x\right) \cdot (\epsilon_v - \epsilon_h) \cdot cos^2\theta \qquad \text{Equation 5-4}$$

In the equation above $\epsilon_v = 2 \cdot \epsilon_h$, x can be c, w, or s, which represent cold space, warm load or earth scene respectively. The reflector emission correction equations for antenna temperature at each of the Earth scene FOV positions is given below:

$$R'_a = C_0 + C_1 \cdot R_a \,. \qquad \text{Equation 5-5}$$

In the equation above, C_0 and C_1 are correction coefficients and can be calculated from reflector emissivity and reflector temperature as below:

For Q_v channels

$$C_0 = \frac{-R_{rfl} \cdot \epsilon \cdot \left(1 + (1-\epsilon)\right) sin^2\theta}{(1-\epsilon) \cdot (1 - \epsilon sin^2\theta)} \qquad \text{Equation 5-6}$$

$$C_1 = \frac{1}{(1-\epsilon)\cdot(1-\epsilon sin^2\theta)}$$ Equation 5-7

For Q_h channels

$$C_0 = \frac{-R_{rfl}\cdot\epsilon\cdot\big(1+(1-\epsilon)\big)cos^2\theta}{(1-\epsilon)\cdot(1-\epsilon cos^2\theta)}$$ Equation 5-8

$$C_1 = \frac{1}{(1-\epsilon)\cdot(1-\epsilon cos^2\theta)}.$$ Equation 5-9

5.4 Antenna Pattern Correction Data

For ATMS, the observed antenna temperature is the convolution between the antenna pattern and the incoming radiation from different sources, including the polarized Earth scene in the main beam, and cold space in the side lobes. The antenna pattern correction needs to be applied in the calibrated antenna temperature. The corrected scene brightness temperature Tb can be derived from the equation below [2]:

$$Tb = A \cdot Ta + B \cdot Tc$$ Equation 5-10

Where Ta is the calibrated antenna temperature, Tc is the cosmic background brightness temperature. The correction coefficients A and B can be calculated from the antenna pattern data as below:

$$A = \frac{1}{\eta^{pp}+n^{pq}}$$ Equation 5-11

$$B = \frac{-\eta_c}{\eta^{pp}+n^{pq}}$$ Equation 5-12

The parameters η^{pp}, η^{pq}, and η^{c} are the Earth scene co-polarization coefficient, Earth scene cross-polarization coefficient, and the cold space spill over combined co- and cross-polarization coefficients, respectively. They are defined as follows:

$$\eta^{pp} = \frac{\int_{\Omega_{ME+SE}} G_{pp}(\theta,\phi)d\theta d\phi}{G_{total}}$$ Equation 5-13

$$\eta^{pq} = \frac{\int_{\Omega_{ME+SE}} G_{pq}(\theta,\phi)d\theta d\phi}{G_{total}}$$ Equation 5-14

$$\eta^{c} = \frac{\int_{\Omega_C}\big(G_{pp}(\theta,\phi)+G_{pq}(\theta,\phi)\big)d\theta d\phi}{G_{total}}.$$ Equation 5-15

Where G_{pp} and G_{pq} are the measured co-pol and cross-pol antenna pattern. The integration angle range is defined by Ω in the equation. For η^{pp} and η^{pq}, it is integrated over the Earth boundary, for η^{c} it is integrated over the cold space. The Earth boundary and integration angle for cold space are determined by the Earth interception angles and the satellite blockage angles, which are derived from the constant scan test during post launch tests; G_{total} is defined as the far-field antenna pattern integrated over areas that are clear of satellite and instrument blockage:

$$G_{total} = \int_{\Omega_{ME+SE+C}} \Big(G_{pp}(\theta,\phi) + G_{pq}(\theta,\phi)\Big)\, d\theta d\phi.$$ Equation 5-16

The Antenna Pattern Correction (APC) coefficients for QS are included in Appendix B.

6. IN-FLIGHT HOT CALIBRATION

The internal calibration targets are approximately cylindrical in outline and are made up of pyramid shaped metal structures coated with an absorbing material. There are two separate targets for K/Ka/V band and W/G band. The aperture of the calibration target for K/Ka/V band is 200cm by 200cm, and 124cm by 124cm for W/G band. For the larger aperture, the pyramids are about 1 cm across and about 4 cm high. The metal base and core ensure that temperature gradients across the targets are minimal, while the pyramid structure and the absorbing coating ensure that the emissivity is close to 1. The target is surrounded by a metal shroud, which mates very closely with a matching shroud surrounding the rotating reflector antenna to prevent stray radiation from external sources from affecting the warm calibration measurements. The targets are not thermally controlled but insulated from the external thermal swings. The peak-to-peak temperature variation within one orbit is expected no more than 0.5K, and no more than 1K during a day. The physical temperatures of the targets are measured by the PRTs in the target, there are 8 of them for K/Ka/V bands and 7 of them for W/G bands. For ATMS on-orbit calibration, three major correction terms are included to reduce the bias in calculated radiance and brightness temperature of the warm targets. These corrections terms are needed for both radiance calibration and brightness temperature calibration.

6.1 Warm Target Correction: Radiance Calibration

The corrections for the radiance of the warm target are dependent on the following three terms: warm load emissivity $\Delta R_{w,em}$, physical temperature $\Delta R_{w,temp}$ and external radiation $\Delta R_{w,cp}$, and the reflector emission term $\Delta R_{w,rfl}$:

$$\Delta R_w = \Delta R_{w,em} + \Delta R_{w,temp} + \Delta R_{w,cp} + \Delta R_{w,rfl} \qquad \text{Equation 6-1}$$

In radiance calibration, the correction terms are firstly calculated as brightness temperature, then transferred to radiance following the methods described in section 2.2.

6.2 Warm Target Correction: Brightness Temperature Calibration

The correction for the brightness of the warm target is calculated from the equation below:

$$\Delta T_w = \Delta T_{w,em} + \Delta T_{w,temp} + \Delta T_{w,cp} + \Delta T_{w,rfl} \qquad \text{Equation 6-2}$$

The correction terms for warm load emissivity, physical temperature measurement bias, the external coupling error, and the reflector emission correction are calculated as brightness temperature.

6.3 Warm load Emissivity Correction

The warm target used in ATMS on-orbit calibration is not a perfect blackbody, the emitted radiation is less than the value computed from the Planck function, resulting in a difference of

$$\Delta T_{w,em} = (\epsilon - 1) \cdot T_w$$ Equation 6-3

Where T_w is the physical temperature of warm target measured by PRTs. For ATMS, its warm target effective emissivity is listed in Table 6.1.

6.4 Warm load temperature error correction

The uncertainty of the warm target radiance, $\Delta T_{w,temp}$, depends on temperature drifts, temperature gradients, and temperature measurement accuracy. Temperature drift is the target temperature change between the time of radiometric observation and the time the physical temperature is measured. For ATMS, the maximum time delay is 2.6667 seconds (the scan period), and the maximum thermal drift rate is about 0.001 K/sec. Thermal analyses indicate that the maximum rate, which occurs at the eclipse in a beta angle (angle between sun vector and orbit plane) of 80 degrees orbit, will be no greater than this rate. In the actual ATMS design, the physical temperature measurements are centered at the same time as the warm calibration radiometric measurements. Therefore, for the nominal-case error budget, this item is reduced to a negligible contribution.

The temperature spatial gradient of the warm target is no greater than 0.2K (Figure 6-1). The use of multiple temperature sensors at different locations allows for an averaging that reduces gradients.

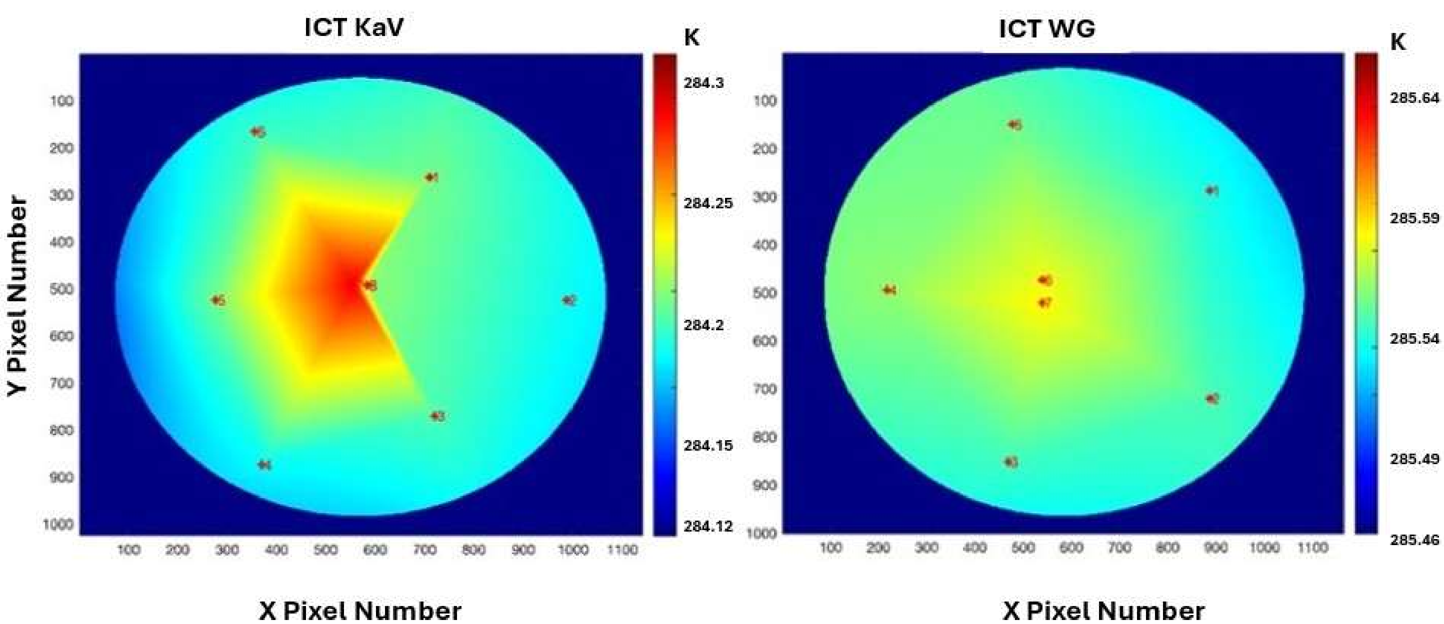

Figure 6-1: Temperature gradient in QS ATMS KaV and WG internal calibration targets (ICT) measured during the instrument TVAC test at scene temperature of 280K and cold plate temperature of 25°C. (To be updated by using the on-orbit data)

The temperature measurement accuracy pertains to the accuracy of the PRTs and their associated read-out electronics. The single four-wire PRT accuracy is about 0.10 K. The averaging of readings from 7 PRTs (minimum required for each calibration target) will reduce the error, but the reduction factor is largely unknown since some of the error terms may be partially correlated.

6.5 Coupling Error Correction

The external radiation is caused by the imperfect coupling of the reflector/shroud assembly to the warm load. The error due to this coupling is given by:

$$\Delta T_{w,ex} = C_g(T_w - T_{ex}) \qquad \text{Equation 6-4}$$

where C_g is the coupling factor, and T_w and T_{ex} are the radiance of warm load and external environment, respectively. With an average on-orbit brightness temperature of the warm load and the external environment, the coupling loss in QS ATMS warm load is calculated and listed in Table 6.1: Warm Target Emissivity and Coupling Loss

Table 6.1: Warm Target Emissivity and Coupling Loss

Channel	**Warm Target Emissivity**	**Coupling Loss(K)**
1	0.9999803	-0.1428
2	0.9999773	-0.1428
3	0.9999972	-0.1212
4	0.9999972	-0.1212
5	0.9999972	-0.1212
6	0.9999927	-0.1212
7	0.9999927	-0.1212
8	0.9999927	-0.1212
9	0.9999927	-0.1212
10	0.9999940	-0.1212
11	0.9999940	-0.1212
12	0.9999940	-0.1212
13	0.9999940	-0.1212
14	0.9999940	-0.1212
15	0.9999940	-0.1212
16	0.9999828	-0.0801
17	0.9999872	-0.0522
18	0.9999866	-0.0522
19	0.9999866	-0.0522
20	0.9999968	-0.0522
21	0.9999968	-0.0522
22	0.9999968	-0.0522

6.6 Reflector Thermal Emission Correction

The ATMS scanning reflector is made of beryllium with a nickel interfacing layer and gold plating. Due to microscopic roughness, the rotating flat reflector is not lossless and has its own thermal emission. For on-orbit calibration, the warm calibration radiances need to be corrected for reflector emission following Equation 5-3 and Equation 5-4, by using the reflector emissivity listed in Table 5.3.

7. IN-FLIGHT COLD CALIBRATION

For ATMS on-orbit calibration, the cold space observations samples are made available through the deep space scan with the selected scan profile that has minimum Earth contamination. As shown in Figure 4-1, the antenna reflectors rotate continuously counterclockwise relative to the spacecraft direction of motion (i.e. the spin vector points in the negative x-direction while the spacecraft moves along the positive x-direction), completing three revolutions in 8 seconds.

Compared to the warm calibration targets, the cold space views are more vulnerable to the contamination from different sources. For brightness temperature calibration based on the modified R-J approximation, the Earth and Spacecraft contamination correction are provided in the data packet for users to apply in their calibration process. For radiance calibration, three major corrections are provided, which include the Earth and spacecraft contamination correction, the Lunar intrusion correction, as well as the reflector emission correction. Note that the model and parameters for corrections of lunar intrusion and reflector thermal emission included in this document can also be adapted for brightness temperature calibration algorithm at user's option.

7.1 Earth and Spacecraft Contamination Correction

The Earth contamination bias is derived using percent energy contributions from the sidelobes and considerations for Earth and spacecraft contributions to sidelobe energy. The expected percentage contributions are provided in Table 7.1. Table 7.1 indicates the biases for each channel band; the last column provides the offset terms, for five bands, which have entries as shown in ATMS Calibration Data Packet, words 68 through 72. Note that the cold calibration offset values are programmed into ATMS EEPROM.

Table 7.1: Predicted Cold Calibration Errors

CH	Earth Intercept		Spacecraft Intercept		Computed Cold Bias (K)	Cold Target Offset Term (K)
	Percent Energy	Error (K)	Percent Energy	Error (K)		
1	0.4622	0.8781	0.0109	0.0100	0.8881	0.8881
2	0.4622	0.8781	0.0109	0.0100	0.8881	0.8881
3-15	0.4962	1.1288	0.0029	0.0027	1.1314	1.1314
16	0.5591	1.2860	0.0002	0.0002	1.2862	1.2862
17	0.2367	0.6154	0.0002	0.0002	0.6156	
18-22	0.1768	0.4598	0.0005	0.0005	0.4603	0.4603

Where: Computed Bias = Earth Error + Spacecraft Error [Bias to cold calibration observation]

For current operational QS ATMS on-orbit calibration algorithm, the Earth and Spacecraft contamination biases listed in Table 7.1 are added to the 2.73K cosmic background brightness temperature, then converted into cold space radiance for calibration.

For users with brightness temperature calibration algorithm based on the modified Rayleigh-Jeans approximation, the cold biases are directly added to the adjusted cold space brightness temperature at different channels for calibration.

7.2 Lunar Intrusion Correction

In the ATMS calibration process, a Lunar Intrusion (LI) event is defined as an occurrence when the Moon disk enters the ATMS main antenna beam during a space view. When the Moon appears in the satellite observation field of view (FOV), the effective microwave brightness temperature of the Moon disk, $\mathrm{TB}^{\mathrm{Ref}}_{\mathrm{Moon}}$can be written as a function of the antenna response function G_{ant}, normalized solid angle of the Moon Ω_{Moon}, and average brightness temperature of the Moon disk TB^{disk}_{Moon} as below:

$$TB^{ref}_{Moon} = \Omega_{moon} \cdot G_{ant} \cdot TB^{disk}_{Moon} \qquad \text{Equation 7-1}$$

In equation 7-1, Ω_{Moon} is the normalized Moon solid angle. The average brightness temperature of the Moon disk is a function of Moon phase angle, and can be calculated from the equation below [3]:

$$Tb^{disk}_{Moon} = 100.89 + 85.65 \cdot (1 - cos\Theta) - 0.24 \cdot (1 + cos2\Theta) \qquad \text{Equation 7-2}$$

Where Θ is the Moon phase angle.

Assuming the azimuthal asymmetry is insignificant, the antenna response within the main beam range can then be accurately simulated by a one-dimensional Gaussian function,

$$G_{ant}(\alpha) = e^{\frac{-(\alpha-\alpha_0)^2}{2\cdot\sigma^2}} \qquad \text{Equation 7-3}$$

where α is the separation angle between antenna boresight and the Moon-in-View vector, α_0 is beam pointing error, and σ is the antenna parameter defined as function of 3 dB beam width θ_{3dB} as

$$\sigma = \frac{0.5\cdot\theta_{3dB}}{\sqrt{2log2}}. \qquad \text{Equation 7-4}$$

The parameters for LI corrections are listed in Table 7.2.

Table 7.2: Lunar Intrusion Correction Parameters (To be updated after PostLaunchTest)

Channel	Ω_{Moon}	α_0	σ
1	0.0062	0.1835	2.2
2	0.0062	0.312	2.23
3	0.0318	0.0959	0.93
4	0.0313	0.118	0.93
5	0.0316	0.1144	0.93
6	0.0316	0.143	0.91
7	0.0319	0.1316	0.91
8	0.0327	0.0752	0.93
9	0.0323	0.1268	0.9
10	0.0337	0.1236	0.89
11	0.0338	0.1227	0.89
12	0.0341	0.1102	0.89

Channel	Ω_{Moon}	α_0	σ
13	0.0336	0.1313	0.89
14	0.0335	0.1368	0.89
15	0.0343	0.1133	0.89
16	0.0339	0.1462	0.86
17	0.0953	0.1256	0.47
18	0.1004	0.0964	0.48
19	0.1	0.097	0.48
20	0.0987	0.1178	0.47
21	0.0989	0.1142	0.47
22	0.0988	0.1165	0.47

For on-orbit radiance calibration, the lunar intrusion correction term is calculated from Equation 7-1, following the LI correction algorithm described in [4].

7.3 Reflector Thermal Emission Correction

The ATMS scanning reflector is made of beryllium with a nickel interfacing layer and gold plating. Due to microscopic roughness, the rotating flat reflector is not lossless and has its own thermal emission. For on-orbit calibration, the cold calibration radiances need to be corrected for reflector emission following Equation 5-3 and Equation 5-4, by using the reflector emissivity listed in Table 5.3.

8. RADIOMETRIC PERFORMANCE AND CALIBRATION

Radiometric performance of the QS ATMS SN 301 instrument can be assessed through on-orbit measurements, thermal vacuum (TVAC) testing, and mathematical modeling. In this section, the instrument's radiometric performance is characterized by temperature sensitivity, non-linearity, and radiometric accuracy. Temperature sensitivity, reported as noise equivalent delta temperature (NEDT), is obtained via on-orbit measurements of the warm internal calibration target (ICT) and cold space views. Non-linearity is measured during TVAC. Radiometric accuracy is determined by measurements taken during TVAC and a mathematical model of the sensor performance which accounts for multiple sources of error.

The remainder of this section is organized as follows. The on-orbit NEDT computation and performance analysis is described first. Next, a brief overview of TVAC testing is provided. The instrument non-linearity parameter is then described and measurements from TVAC are presented. Finally, a description of the instrument performance model is provided along with derived estimates of on-orbit accuracy.

8.1 On-Orbit Temperature Sensitivity

NEDT is a measure of the noise power in each channel of the instrument. Specifically, it is the standard deviation of calibrated temperature measurements at a given scene temperature in K. It is generally considered the smallest change in brightness temperature detectable by the instrument.

8.1.1 Sensor Data Record Calculation

On-orbit NEDTs corresponding to the warm load and cold space views for each channel are reported in the sensor data record (SDR). The calculated on-orbit NEDT includes all sources of noise, including white and flicker noise. The NEDT calculation is described in the *Joint Polar Satellite System Algorithm Specification Volume III: Operational Algorithm Description (OAD) for the ATMS RDR/TDR/SDR* (474-00448-03-02) (https://www.nesdis.noaa.gov/about/documents-reports/jpss-technical-documents/jpss-science-documents). It will be briefly summarized here.

For each scan, 4 warm load and 4 cold space views are used to compute warm and cold scan-level NEDTs. The NEDT for a particular channel at the current scan is given by

$$NEDT = \sqrt{\frac{1}{2M-1}\sum_{j=1}^{M}\sum_{i=1}^{2}\left(NW_{i,j} - \overline{NW}\right)^2} \qquad \text{Equation 8-1}$$

Where $NW_{i,j} = TA_{i,j}^{W} - \overline{TW}_j$ and $TA_{i,j}^{W}$ is the calibrated brightness temperature at pixel i (4 in total) and scan j. The number of along track scans used for averaging is M=10. The NEDT computation is identical for each channel; thus, no subscripts are used in this section to denote channel. Calibrated brightness temperatures $TB_{i,j}^{W}$ are given by Equation 8-2 and $\overline{TW}_j$ is given by Equation 8-3. The quantity $\overline{NW}$ is the average of the $NW_{i,j}$ used in Equation 8-1. Similar equations are used for the cold space NEDT. For the warm load NEDT,

$$TB_{i,j}^{W} = \frac{1}{\bar{G}_j}\left(CW_{i,j} - \overline{CC}_j\right) + TC,\ 1 \le i \le 2,\ 1 \le j \le n_{scan} \qquad \text{Equation 8-2}$$

and the average warm load temperature

$$\overline{TW}_k = \frac{1}{N_{PRT}(2n+1)}\sum_{j=k-n}^{k+n}\sum_{i=1}^{N_{PRT}} TW_{i,j} \qquad \text{Equation 8-3}$$

where k is the index of the current scan, n is equal to half the number of scans used in warm load smoothing (n=4 in operational algorithm), N_PRT is the number of warm load PRT temperature readings (N_PRT=8 for K-, Ka-, and V-bands, N_PRT=7 for W- and G-bands). The quantities CW and CC are warm and cold counts, respectively. The quantity TC=2.73 K is the cold space brightness temperature.

The cold space NEDT is similarly given by Equation 8-1 with $NW_{i,j} = TB_{i,j}^{C} - TC$, where $TB_{i,j}^{C}$ are the calibrated brightness temperatures for the cold space view, given by

$$TA_{i,j}^{C} = \frac{1}{\bar{G}_j}\left(CC_{i,j} - \overline{CC}_j\right) + TC,\ 1 \le i \le 2,\ 1 \le j \le n_{scan} \qquad \text{Equation 8-4}$$

the quantity $\overline{NW}$ is the average of the $NW_{i,j}$.

The calibration gain used in the NEDT calculations is given by

$$\bar{G}_j = \frac{\overline{CW}_j - \overline{CC}_j}{\overline{TW}_j - TC} \qquad \text{Equation 8-5}$$

$$\overline{CW}_k = \frac{1}{2(2n+1)}\sum_{j=k-n}^{k+n}\sum_{i=3}^{4} CW_{i,j} \qquad \text{Equation 8-6}$$

$$\overline{CC}_k = \frac{1}{4(2n+1)}\sum_{j=k-n}^{k+n}\sum_{i=1}^{4} CC_{i,j} \qquad \text{Equation 8-7}$$

The value N is the number of along track scans to use for averaging cold counts. The value N=4 for all channels except 17, 21 and 22, for which N=2.

8.1.2 Extrapolation to 300 K Scene Temperature

The channel NEDT depends on the calibration target temperature. This is either the warm load (nominally ~280 K), or cold space (2.73 K). The NEDT performance requirement for the instrument is specified at a scene temperature of 300 K. To demonstrate on-orbit NEDT performance against this requirement, the NEDT for a 300 K scene temperature is estimated by extrapolating the on-orbit warm and cold NEDTs to a 300 K scene. The i-th NEDT estimate is given by the linear extrapolation

$$NEDT_{300,i} = \frac{\overline{NEDT}_{C,i} - \overline{NEDT}_{W,i}}{T_C - \bar{T}_i}(300 - T_C) + \overline{NEDT}_{C,i}$$ Equation 8-8

where $\overline{NEDT}_{C,i}$ is an average cold NEDT, $\overline{NEDT}_{W,i}$ is an average warm NEDT, $\bar{T}_i$ is an average warm load temperature, and $T_C = 2.73\ K$ is the cold space temperature. The warm load temperature is available in the Raw Data Record (RDR).

A representative set of on-orbit 300 K NEDT values from xxxx 2026 are shown in Table 8.1 and maximum values are depicted in Figure 8-1. These results were computed using the first orbit of each day of the month with the following procedure:

1. Retrieve NEDT and calibration target temperatures from SDR and RDR files from the first orbit of each day of the month.
2. Compute the i-th average cold $\overline{NEDT}_{C,i}$ and warm $\overline{NEDT}_{W,i}$ for each SDR file (nominally 180 scans), excluding data fill values (DFVs) and statistical outliers, by taking the root mean square of every M-th NEDT value in the SDR. M=10 is as defined in Section 8.1.1, to avoid overlapping brightness temperatures in NEDT values. The average warm and cold NEDT values are thus given by

$$\overline{NEDT}_{*,i} = \sqrt{\frac{M}{180}\sum_{j=1}^{180/M} NEDT^2_{*,i,(j-1)\times M+1}}$$ Equation 8-9

   Where $NEDT_{*,i,k}$ is the NEDT value for the k-th scan of the i-th SDR file and * may be either W for warm or C for cold.
3. Compute one $NEDT_{300,i}$ for each SDR file using equation 8-8 with the average cold and warm NEdT from step 1 and average ICT temperatures.
4. Compute the average and maximum over all $NEDT_{300,i}$ for the month

The maximum on-orbit 300 K NEdT values are shown in Figure 8-1.

Table 8.1: QS ATMS On-Orbit NEdT (from TVAC, to be updated Post-Launch)

Channel	*Attribute (K)*	*Max. (K)*	*Mean (K)*	*Std. (K)*
1	**0.70**	**0.268**	0.265	0.003
2	**0.80**	**0.546**	0.533	0.013
3	**0.90**	**0.547**	0.522	0.019
4	**0.70**	**0.457**	0.432	0.021
5	**0.70**	**0.407**	0.393	0.012
6	**0.70**	**0.408**	0.398	0.011
7	**0.70**	**0.397**	0.390	0.006
8	**0.70**	**0.409**	0.403	0.005
9	**0.70**	**0.423**	0.418	0.005
10	**0.75**	**0.511**	0.497	0.010
11	**1.20**	**0.630**	0.620	0.009

Channel	Attribute (K)	Max. (K)	Mean (K)	Std. (K)
12	1.20	**0.668**	0.661	0.008
13	1.50	**0.951**	0.932	0.014
14	2.40	**1.292**	1.267	0.031
15	3.60	**2.017**	1.989	0.028
16	0.50	**0.505**	0.491	0.015
17	0.60	**0.589**	0.567	0.017
18	0.80	**0.350**	0.346	0.005
19	0.80	**0.396**	0.388	0.008
20	0.80	**0.446**	0.439	0.007
21	0.80	**0.488**	0.472	0.016
22	0.90	**0.618**	0.614	0.003

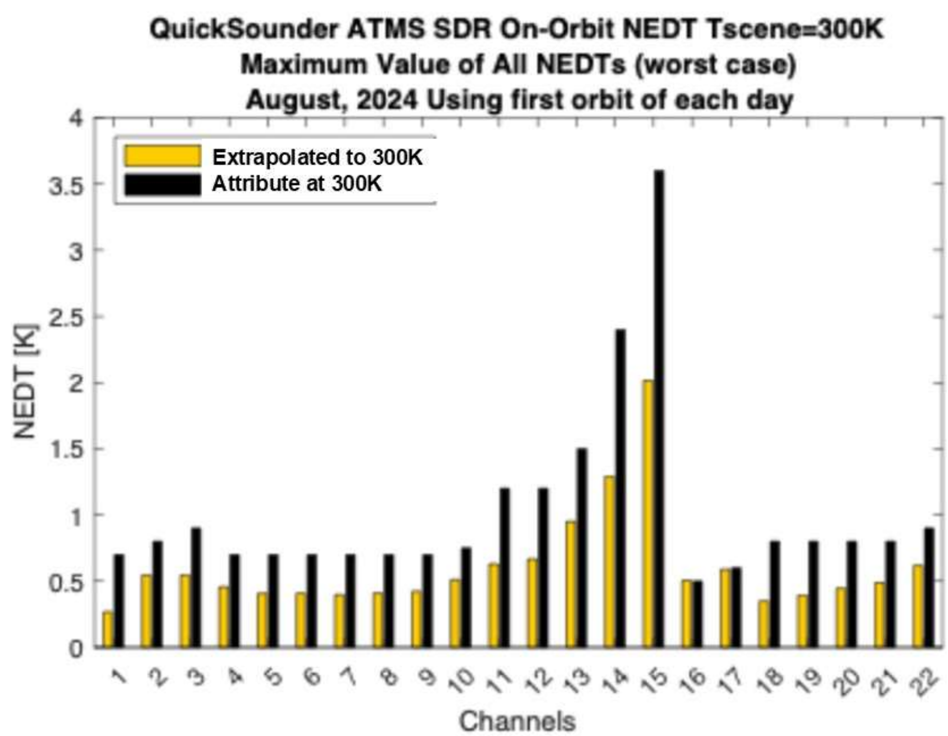

Figure 8-1: QS ATMS Maximum On-Orbit NEDT (from TVAC. To be updated Post-Launch)

8.2 Thermal Vacuum Testing

Radiometric performance of the QS ATMS SN 301 instrument is assessed during TVAC testing. The primary purpose of TVAC testing is to characterize the performance of the instrument in terms of temperature sensitivity (NEDT), calibration accuracy, and linearity. The instrument performance is assessed in a vacuum chamber at <1 x 10^{-5} Torr at a series of instrument and simulated scene temperatures. The profile of instrument and scene temperatures achieved during TVAC is provided in Figure 8-2.

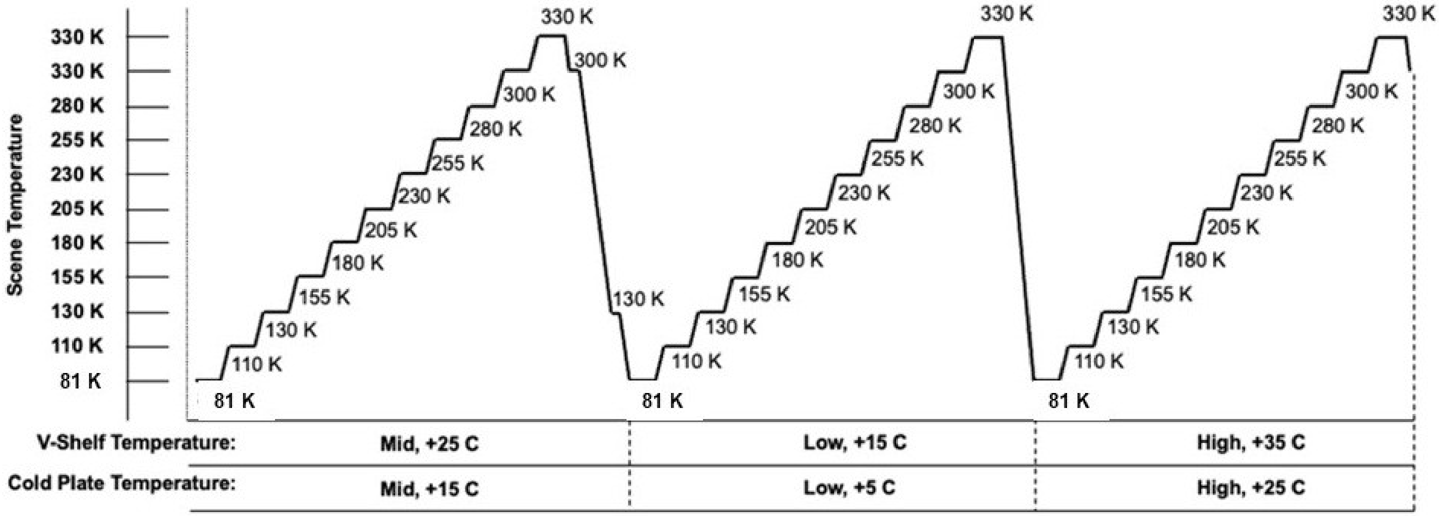

Figure 8-2: TVAC Calibration Instrument and Scene Temperature Profile

The instrument cold plate (CP) is cycled through three temperature plateaus, to simulate the expected lowest (CP Low: +5 C), nominal (CP Mid: +15 C), and highest (CP High: +25 C) operating temperatures of the instrument. At each CP plateau, an external variable temperature blackbody scene target is cycled through 11 scene temperatures. The scene temperature is measured and controlled to within 0.1 K. The temperatures are chosen to span the range from 81 K (lowest practically achievable scene temperature) to 330 K (highest expected scene temperature during operation). On-orbit, the lowest scene temperature is 2.73 K, which is encountered during the cold space view of calibration. For non-linearity analysis, the instrument transfer function is extrapolated to include 3 K (≅ 2.73 K). For the midpoint cold plate temperature at + 15 C, while TVAC calibration tests were performed at each scene temperature, ATMS collects 278 scans of the scene target at each of 4 redundancy configurations (RCs) 1, 2, 5, and 6, see Table 8.2. For the operational high and low cold plate temperatures, only RCs 1 and 2 were tested. The radiometric data and variable scene target temperatures can then be used to determine temperature sensitivity (NEDT), accuracy, and linearity.

Table 8.2: Instrument Redundancy Configurations (RCs)

RC Number	Instrument Configuration
1	A-Side of PLO, B-side of LOs, A-side of RPS, A-side of SPA, A-side of SDE; and SAW-A
2	A-Side of PLO, B-side of LOs, A-side of RPS, A-side of SPA, A-side of SDE; and SAW-B
5	B-Side of PLO, B-side of LOs, B-side of RPS, B-side of SPA, B-side of SDE; and SAW-B
6	B-Side of PLO, B-side of LOs, B-side of RPS, B-side of SPA, B-side of SDE; and SAW-A

8.3 Non-Linearity

Nonlinearity parameters are derived from the ground Thermal Vacuum Test. The algorithms being used to derive the nonlinearity parameters are different for brightness temperature calibration based on modified R-J approximation and the radiance calibration based on the Planck function. Accordingly, the nonlinearity parameters for radiance calibration and the modified R-J based brightness temperature calibration are provided separately and should be used consistently with the corresponding calibration algorithm the user chooses.

8.3.1 Nonlinearity Characterization in Brightness Temperature

The transfer function of the ATMS radiometer describes how the calibrated brightness temperatures at the instrument output vary with the true scene brightness temperatures. A linear transfer function is ideal; however, ATMS exhibits a quadratic non-linearity. The two-point calibration effectively fits a linear approximation to this function; thus, there is residual error in the calibrated brightness temperatures due to non-linearity. This non-linearity is determined from TVAC measurements and corrected in ground processing algorithms.

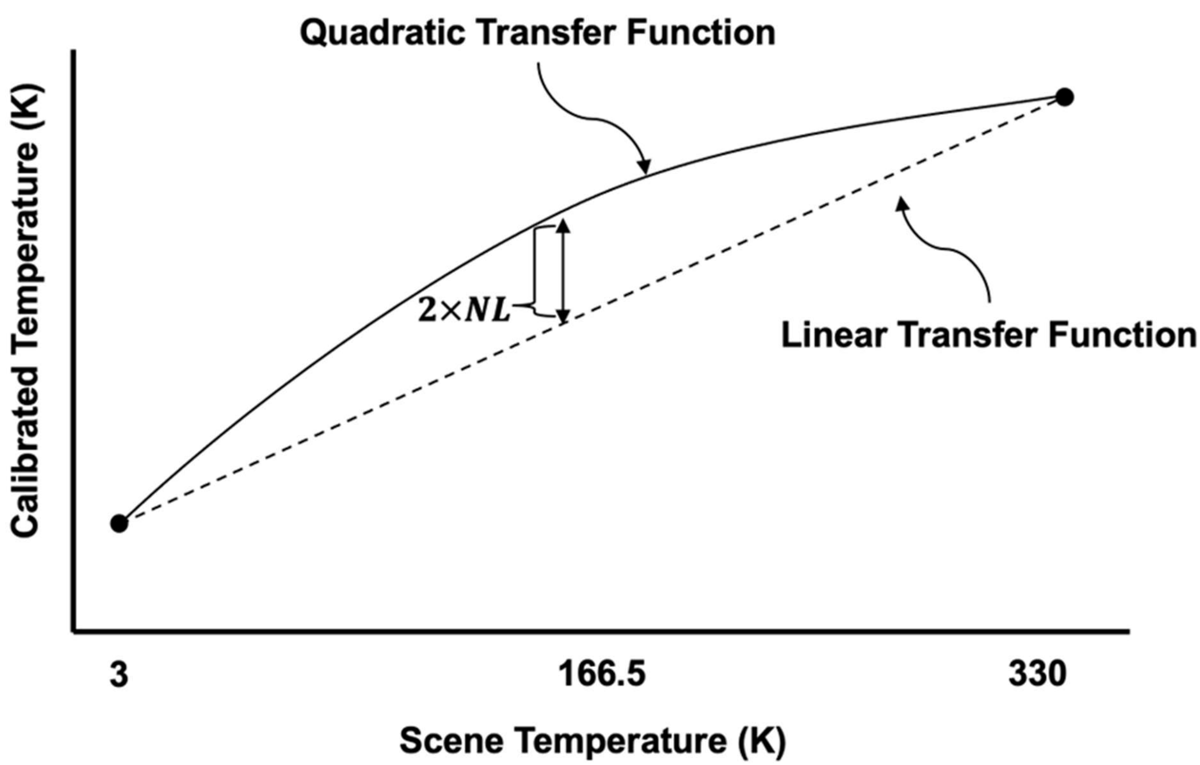

Figure 8-3: Transfer Function in Brightness Temperature

On-orbit non-linearity (NL) is defined as one half the maximum difference between a quadratic regression curve, fit to the calibration accuracy, and a linear fit over the dynamic range of the instrument (3-330 K). An illustration of the NL metric is depicted in Figure 8-3. Specifically, calibration accuracy at scene temperature i is given by

$$\Delta T_i = T_i - \hat{T}_i \qquad \text{Equation 8-10}$$

where T_i is the true measured scene temperature and $\hat{T}_i$ is the ATMS calibrated brightness temperature. A quadratic regression curve is fit the ΔT_i's, denoted

$$f_{quad}(T) = a_0 + a_1 T + a_2 T^2 \qquad \text{Equation 8-11}$$

where a_0, a_1, and a_2 are polynomial coefficients that specify the quadratic regression curve, and T is an arbitrary scene temperature. The non-linearity is extrapolated to the dynamic range of the instrument to obtain $f_{quad}(3)$ and $f_{quad}(330)$. A linear function is obtained as a line intersecting the two extremes

$$f_{lin}(T) = \frac{f_{quad}(330) - f_{quad}(3)}{330-3}(T-3) + f_{quad}(3)$$ Equation 8-12

The NL is thus obtained

$$NL = \frac{1}{2}\left(f_{quad}(T = 166.5) - f_{lin}(T = 166.5)\right)$$ Equation 8-13

where $T = 166.5$ is the halfway point of the instrument dynamic range, the temperature where the non-linearity is maximum.

Non-linearities for each channel, and RC are listed in Table 8.3. The "Std. Dev." column is the standard deviation of non-linearity values for each CP temperature. The residual uncertainty is the maximum standard deviation across all RCs and CP temperatures, denoted ΔNL.

Table 8.3: Worst-Case Non-Linearity and Residual Uncertainties

Channel	Low			Mid					High			Residual Uncertainty (K)
	RC1 (K)	RC2 (K)	Std. Dev. (K)	RC1 (K)	RC2 (K)	RC5 (K)	RC6 (K)	Std. Dev. (K)	RC1 (K)	RC2 (K)	Std. Dev. (K)	
1	0.797	0.786	0.008	0.732	0.754	0.740	0.751	0.010	0.712	0.716	0.003	0.010
2	0.523	0.491	0.022	0.457	0.463	0.484	0.433	0.021	0.471	0.447	0.017	0.021
3	0.312	0.309	0.002	0.324	0.296	0.319	0.297	0.015	0.306	0.285	0.015	0.015
4	0.339	0.340	0.001	0.321	0.301	0.350	0.325	0.020	0.341	0.305	0.026	0.020
5	0.327	0.325	0.001	0.331	0.300	0.335	0.316	0.016	0.326	0.312	0.010	0.016
6	0.414	0.406	0.006	0.403	0.387	0.418	0.390	0.014	0.401	0.398	0.002	0.014
7	0.472	0.475	0.002	0.477	0.465	0.484	0.451	0.015	0.468	0.462	0.004	0.015
8	0.405	0.411	0.004	0.407	0.402	0.415	0.395	0.008	0.414	0.403	0.008	0.008
9	0.411	0.435	0.017	0.436	0.423	0.429	0.429	0.005	0.437	0.422	0.011	0.005
10	0.452	0.454	0.002	0.428	0.440	0.456	0.436	0.012	0.437	0.415	0.015	0.012
11	0.443	0.445	0.002	0.442	0.409	0.440	0.423	0.016	0.435	0.401	0.024	0.016
12	0.425	0.423	0.001	0.432	0.395	0.411	0.409	0.015	0.431	0.400	0.022	0.015
13	0.360	0.382	0.016	0.365	0.375	0.408	0.415	0.025	0.405	0.356	0.034	0.025
14	0.366	0.407	0.029	0.424	0.410	0.458	0.378	0.033	0.384	0.445	0.043	0.033
15	0.308	0.402	0.066	0.395	0.420	0.303	0.256	0.077	0.374	0.387	0.009	0.077
16	0.386	0.346	0.028	0.388	0.400	0.370	0.416	0.019	0.365	0.377	0.008	0.019
17	0.388	0.397	0.006	0.407	0.379	0.405	0.434	0.023	0.355	0.395	0.028	0.023
18	0.367	0.368	0.000	0.388	0.378	0.390	0.393	0.007	0.346	0.357	0.007	0.007
19	0.405	0.391	0.010	0.412	0.406	0.413	0.424	0.008	0.391	0.401	0.007	0.008
20	0.385	0.376	0.006	0.430	0.421	0.422	0.394	0.016	0.390	0.390	0.000	0.016
21	0.387	0.373	0.010	0.414	0.399	0.402	0.398	0.007	0.383	0.399	0.011	0.007
22	0.432	0.399	0.023	0.437	0.467	0.450	0.441	0.013	0.413	0.434	0.015	0.013

The calibration accuracy data used to compute the non-linearity parameters and uncertainty is collected during TVAC. The calibration accuracy data is included in Appendix C and the non-linearity data, including regression coefficients and NL parameters, are included in Appendix D. NL parameters in radiance units are included in Appendix E. Figure 8.4 presents on-orbit non-linearity of QS ATMS in brightness temperature for instrument temperature (Cold Plate) at Low, Mid, and High.

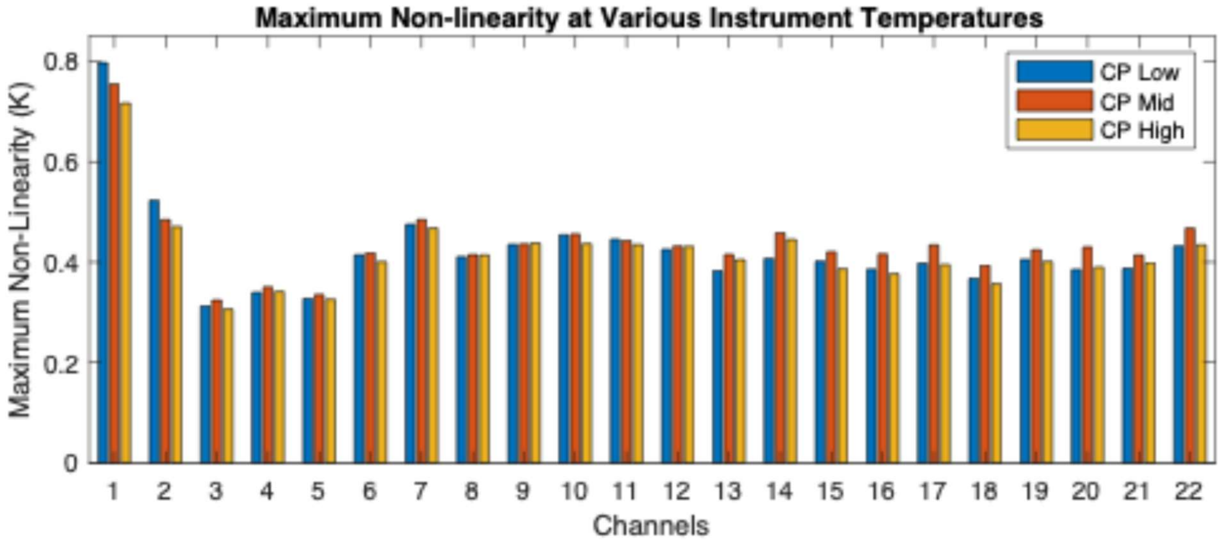

Figure 8-4: Maximum nonlinearity at Mid, Low and High instrument temperature for QS ATMS

For DB users, the nonlinearity parameter μ is calculated in brightness temperature space at instrument temperature of Low (+5° **C**), Middle (15° **C**), and High (25° **C**). The nonlinearity term can be calculated from equation 8-14 as below:

$$Q^T = \mu \cdot (T_w - T_c)^2 x(x-1).$$ Equation 8-14

Where Tw and Tc are the warm load and cold space brightness temperature respectively. μ parameters at different instrument temperature are listed in Table 8.4.

Table 8.4: QS ATMS Nonlinearity μ (K^{-1}) Parameters for DB User (RC1)

Channel	Instrument Cold Plate Temperature 15 C	25 C	35 C
1	5.88E-05	5.64E-05	5.36E-05
2	3.68E-05	3.46E-05	3.34E-05
3	2.31E-05	2.21E-05	2.13E-05
4	2.54E-05	2.25E-05	2.28E-05
5	2.43E-05	2.24E-05	2.33E-05
6	3.04E-05	2.90E-05	2.98E-05
7	3.56E-05	3.48E-05	3.46E-05
8	3.07E-05	3.01E-05	3.01E-05
9	3.26E-05	3.16E-05	3.15E-05
10	3.40E-05	3.29E-05	3.11E-05
11	3.33E-05	3.06E-05	3.00E-05
12	3.17E-05	2.96E-05	2.99E-05

	Instrument Cold Plate Temperature		
Channel	15 C	25 C	35 C
13	2.86E-05	2.80E-05	2.67E-05
14	3.04E-05	3.06E-05	3.33E-05
15	3.00E-05	3.15E-05	2.89E-05
16	2.59E-05	2.99E-05	2.82E-05
17	2.97E-05	2.83E-05	2.96E-05
18	2.75E-05	2.83E-05	2.67E-05
19	2.92E-05	3.03E-05	3.00E-05
20	2.81E-05	3.15E-05	2.92E-05
21	2.79E-05	2.98E-05	2.98E-05
22	2.98E-05	3.50E-05	3.25E-05

Note that for DB users, the following correction should be applied to the nonlinearity parameters A_2 read out from the ATMS Calibration Data Packet, words 73 through 94 when applying Equation 8-14 for the nonlinearity correction:

$$A_2 = -\mu$$

8.3.2 Nonlinearity Characterization in Radiance

Calibration measurements are used to accurately determine the radiometer transfer function, which relates the instrument's digitized output (i.e., counts) to physical radiance. The radiometric calibration for radiance (R) in ATMS is derived as follows:

$$R = R_c + (R_w - R_c) * \frac{(C_s - \bar{C}_c)}{(\bar{C}_w - \bar{C}_c)} + Q^R \qquad \text{Equation 8-15}$$

where:

R_w and R_c are the radiances of the warm and cold calibration targets, corresponding to their mean temperatures T_w and T_c, respectively. $\overline{C_w}$ and $\overline{C_c}$ are the mean warm and cold counts within the calibration sectors. C_s is the scene count. This counts-to-radiance transfer function is illustrated schematically in Figure 8.4. In the figure, subscripts c and w refer to the cold and warm calibration points, respectively, while subscript s refers to an Earth scene.

The nonlinearity parameter, Q^R in Equation 8-15 was estimated using the pre-launch instrument response datasets generated at low, nominal, and high instrument cold plate (CP) temperatures. For ATMS thermal vacuum (TVAC) test data, the scene temperature ranges between 81 K and 330 K with the cold calibration temperature at 81 K. However, for ATMS on-orbit calibration, the cold calibration temperature is approximately 2.73 K (space view sector). Thus, the nonlinearity value must be estimated by extrapolating the TVAC data to 2.73 K. In general, the nonlinear term Q^R can be expressed as a function of nonlinearity parameter μ as below:

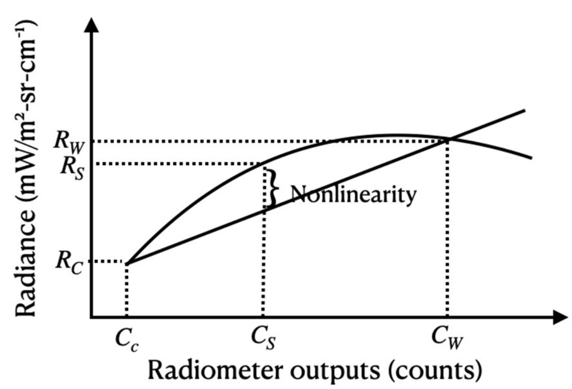

Figure 8-5: Transfer Function in Radiance

$$Q^R = \mu \cdot (R_w - R_c)^2 x(x - 1) \qquad \text{Equation 8-16}$$

where R_w and R_c are the computed radiance from warm and cold calibration target brightness temperatures, and x is the normalized scene counts with

$$x = \frac{C_s - \overline{C_c}}{\overline{C_w} - \overline{C_c}} \quad \text{Equation 8-17}$$

For QS ATMS TVAC test, the nonlinearity parameters are derived for instrument temperature setting at 5°C, 15°C and 25°C to cover the possible on-orbit operational instrument temperature variation range. Then a quadratic function can be used to fit the relationship between the instrument temperature T_{rx} and μ as below:

$$\mu = a_2 \cdot T_{rx}^2 + a_1 \cdot T_{rx} + a_0 \quad \text{Equation 8-18}$$

where a_0, a_1, a_2 are regression coefficients and provided in Appendix E. The nonlinearity term Q^R in Equation 8-15 can also be expressed as a function of maximum nonlinearity R_{nlmax} as:

$$Q^R = R_{nlmax} \cdot [4 \cdot (x - 0.5)^2 - 1] \quad \text{Equation 8-19}$$

where $R_{nlmax} = \frac{1}{4} \cdot \mu \cdot (R_w - R_c)^2$. Figure 8.5 presents maximum on-orbit nonlinearity of QS ATMS in brightness temperature for operational instrument temperature (Cold Plate) of 15°.

8.4 Derived On-Orbit Radiometric Calibration Accuracy

On-orbit radiometric calibration accuracy is an important performance characteristic of the instrument. Three important factors primarily contribute to the calibration accuracy, hot calibration error, cold calibration error, and uncertainty of the non-linearity. By combining these components, the calibration accuracy can be modeled as

$$T_{Acc} = xE_H + (1 - x)E_C + \Delta T_L \quad \text{Equation 8-20}$$

where

$$x = \frac{T_S - T_C}{T_H - T_C} \quad \text{Equation 8-21}$$

$$\Delta T_L = 4x(1 - x)\Delta NL_C \quad \text{Equation 8-22}$$

and

T_{Acc}	: Predicted On-Orbit Calibration Accuracy
T_S	: Scene temperature
T_C	: Cold calibration target temperature
T_H	: Hot calibration target temperature
E_C	: Cold calibration error
E_H	: Hot calibration error
ΔT_{NL}	: Non-linearity error
ΔNL_C	: Residual Non-linearity uncertainty

The term $x = \frac{T_S - T_C}{T_H - T_C}$ can be interpreted as the normalized scene temperature, where $x = 0$ when $T_S = T_C$ and $x = 1$ when $T_S = T_H$. The first term of Equation 8-20, xE_H, is thus the amount the hot calibration error that contributes to the overall calibration error, which increases as T_S approaches T_H. Similarly, the term $(1 - x)E_C$ reflects the error due to cold calibration, which increases as T_S approaches T_C. The non-linearity term $4x(1 - x)T_{NL}$ peaks at the midpoint between T_C and T_H, where the transfer function non-linearity is maximum.

8.4.1 Hot Calibration Error

The hot calibration error is due to the emissivity of the calibration targets, temperature gradients across the calibration targets, temperature measurement accuracy, and RF coupling to the reflector. For the worst-case analysis, the measured emissivity of 0.9999 was used to compute the hot calibration error. The temperature spatial gradient is specified to be no greater than $\pm 0.050\ K$, and this value is used in the worst-case analysis. The temperature sensor PRT accuracy is set to the specified value of $0.10\ K$. Reflector coupling error is the result of receiver external radiation, due to imperfect coupling of the reflector to the hot target because of a gap between the reflector shroud and hot target. ATMS is designed for a 4.75 ± 0.25 mm gap, a value of 5.08 mm was used for the worst-case analysis. The worst-case hot calibration error is listed in Table 8.5.

8.4.2 Cold Calibration Error

The cold calibration error is due to uncertainty in the cosmic background temperature and radiation from the earth and spacecraft during the cold space view through antenna sidelobes. A maximum energy contribution from the antenna sidelobes is specified and this value is used for worst-case analysis. The worst-case cold calibration error is listed in Table 8.5.

8.4.3 Non-Linearity Uncertainty Error

Uncertainty in the non-linearity contributes error to the radiometer transfer function. Non-linearity of the transfer function is characterized during TVAC and can be corrected in ground processing algorithms; however, there is uncertainty in the estimation of non-linearity parameters. This is captured by the standard deviation of estimated non-linearity parameters, which corresponds to the Residual Uncertainty column of Table 8.5.

The non-linearity parameter is specified as the peak deviation of the estimated error quadratic regression curve over the instrument dynamic range 3-330 K. The peak contribution of non-linearity uncertainty scales with the squared ratio of the expected calibration dynamic range to the instrument dynamic range. The maximum predicted hot calibration target temperature over the lifetime of the instrument is 298 K. The worst-case expected contribution of non-linearity uncertainty is therefore

$$\Delta NL_C = 2 \times \Delta NL \times \left(\frac{298-3}{330-3}\right)^2 = 1.628 \times \Delta NL \qquad \text{Equation 8-23}$$

An additional contributing factor to non-linearity uncertainty is the calibration target temperature errors due to thermal gradients in the target. Allocating $\pm 0.10\ K$ over a uniform distribution for this error source results in a contribution of 0.05774 K. The worst-case calibration accuracies and non-linearity uncertainty errors are listed in Table 8.5.

The worst-case expected calibration accuracies are listed in Table 8.6 for cold, mid, and hot scene temperatures. The cold and hot scene temperatures are chosen to span the expected dynamic range of scene temperatures and the mid is taken as the average. A maximum hot calibration target temperature of 298 K is used. The calibration errors are obtained by applying the calibration accuracy model Equation 8-20 to the given scene temperatures and calibration errors in Table 8.5.

Table 8.5: Worst-case calibration accuracies and non-linearity uncertainty errors (K)

Channel	Hot Cal.	Cold Cal.	Non-linearity
1	0.0767	0.6395	0.0955
2	0.0767	0.6395	0.1008
3	0.0710	0.6722	0.0971
4	0.0710	0.6722	0.1030
5	0.0710	0.6722	0.0976
6	0.0710	0.6722	0.0968

Channel	Hot Cal.	Cold Cal.	Non-linearity
7	0.0710	0.6722	0.0970
8	0.0710	0.6722	0.0949
9	0.0710	0.6722	0.0981
10	0.0710	0.6722	0.0971
11	0.0710	0.6722	0.1017
12	0.0710	0.6722	0.1008
13	0.0710	0.6722	0.1093
14	0.0710	0.6722	0.1176
15	0.0710	0.6722	0.1568
16	0.0723	0.7616	0.1044
17	0.0534	0.7616	0.1044
18	0.0534	0.7616	0.0947
19	0.0534	0.7616	0.0955
20	0.0534	0.7616	0.0974
21	0.0534	0.7616	0.0957
22	0.0534	0.7616	0.1014

Table 8.6: Worst-case calibration accuracies for cold, mid, and hot scene temperatures

Channel	Attribute	Cold		Mid		Hot	
		Scene Temp (K)	Accuracy (K)	Scene Temp (K)	Accuracy (K)	Scene Temp (K)	Accuracy (K)
1	⩽ 1.00	130.0	0.491	190.0	0.371	250.0	0.220
2	⩽ 1.00	130.0	0.496	190.0	0.376	250.0	0.223
3	⩽ 0.75	180.0	0.404	227.5	0.285	275.0	0.146
4	⩽ 0.75	180.0	0.410	227.5	0.289	275.0	0.147
5	⩽ 0.75	180.0	0.405	227.5	0.285	275.0	0.146
6	⩽ 0.75	180.0	0.404	227.5	0.285	275.0	0.146
7	⩽ 0.75	180.0	0.404	227.5	0.285	275.0	0.146
8	⩽ 0.75	180.0	0.402	227.5	0.284	275.0	0.145
9	⩽ 0.75	180.0	0.405	227.5	0.286	275.0	0.146
10	⩽ 0.75	180.0	0.404	227.5	0.285	275.0	0.146
11	⩽ 0.75	180.0	0.409	227.5	0.288	275.0	0.147
12	⩽ 0.75	180.0	0.408	227.5	0.288	275.0	0.147
13	⩽ 0.75	180.0	0.416	227.5	0.294	275.0	0.149
14	⩽ 0.75	180.0	0.424	227.5	0.300	275.0	0.152
15	⩽ 0.75	180.0	0.462	227.5	0.329	275.0	0.163
16	⩽ 1.00	180.0	0.448	230.0	0.305	280.0	0.138
17	⩽ 1.00	225.0	0.306	260.0	0.191	295.0	0.065
18	⩽ 1.00	225.0	0.299	260.0	0.187	295.0	0.064
19	⩽ 1.00	225.0	0.300	260.0	0.187	295.0	0.064
20	⩽ 1.00	225.0	0.301	260.0	0.188	295.0	0.065

Channel	Attribute	Cold		Mid		Hot	
		Scene Temp (K)	Accuracy (K)	Scene Temp (K)	Accuracy (K)	Scene Temp (K)	Accuracy (K)
21	⩽ 1.00	225.0	0.300	260.0	0.187	295.0	0.064
22	⩽ 1.00	225.0	0.304	260.0	0.190	295.0	0.065

9. SPECTRAL RESPONSE FUNCTIONS

9.1 Channel Frequency and Bandpass Characteristics

This section presents the center channel frequency and the bandpass characteristics for all ATMS channels. The measurements of the channel center frequencies at intermediate frequencies (IF) and radio frequencies (RF) are summarized in columns 2 and 3 of Table 9.1, respectively. The associated bandwidth of each channel is presented in the last column of Table 9.1.

Note that channels 1 and 2 are not listed in the second column Table 9.1 as they employ direct detection and therefore operate at RF only.

The measurements of the center frequency and bandwidth were performed at the cold plate mid temperature of + 20°C and nominal bias voltage. Primary and Redundant configurations were also tested. Similar results were obtained in the redundant configuration; therefore, they are not presented in this calibration data book. The change of the channel center frequency with the shelf temperature was also evaluated and shows little variation for all channels. This document only presents the values corresponding to temperatures that are expected to be encountered on orbit.

It should be noted that some of the channel center frequencies were measured at ambient pressure, so they need to be corrected to reflect on-orbit performance as the filter (if not hermetically sealed) behaves differently while in vacuum. The values listed in Table 9.1a and 9.1b are RF and IF center frequencies and bandwidths represent at +20 C and nominal voltage at RC1 (Primary) and RC5 (Redundant), and applied correction to reflect the performance under vacuum.

The measurements of the Spectral Response Functions for all the ATMS channels are detailed in section 9.2 and are available in Appendix F to this calibration data book.

Table 9.1a: Channel Center Frequencies and bandwidth for ATMS Primary Channels

Channel	*IF Center Frequency (MHz)*	*RF Center Frequency (MHz)*	*RF Bandwidth (MHz)*
1	N/A	23800.16	263.69
2	N/A	31404.64	180.30
3	6992.60	50297.68	168.00
4	5526.79	51763.49	361.10
5	4490.26	52800.02	381.10
6a	3581.78	53708.50	157.90
6b	3809.95	53480.33	160.30
7	2890.51	54399.77	371.80
8	2351.39	54938.89	375.70

Channel	*IF Center Frequency (MHz)*	*RF Center Frequency (MHz)*	*RF Bandwidth (MHz)*
9	1791.86	55498.42	313.60
10	87.10	57290.28	326.2
11	217.55	57290.28 ± 217.55	77.50
12a	274.85	57290.28 ± 274.85	35.50
12b	369.60	57290.28 ± 369.60	35.80
13a	300.26	57290.28 ± 300.26	15.75
13b	344.19	57290.28 ± 344.19	15.88
14a	312.21	57290.28 ± 312.21	7.99
14b	332.22	57290.28 ± 332.22	7.99
15a	317.65	57290.28 ± 317.65	2.92
15b	326.59	57290.28 ± 326.59	2.92
16	5456.72	88210.73	1970.00
17	924.40	165508.02	2987.6
18	7012.71	183252.21 ± 7012.71	1949.00
19	4487.91	183252.21 ± 4487.91	1897.00
20	2988.00	183252.21 ± 2988.00	984.00
21	1793.10	183252.21 ± 1793.10	978.60
22	1000.75	183252.21 ± 1000.75	506.70

Table 9.2b: Channel Center Frequencies and bandwidth for ATMS Redundant Channels

Channel	*IF Center Frequency (MHz)*	*RF Center Frequency (MHz)*	*RF Bandwidth (MHz)*
1	N/A	23800.16	263.69
2	N/A	31404.64	180.30
3	6992.75	50297.50	168.30
4	5526.39	51763.86	360.30
5	4489.91	52800.34	381.80
6a	3582.18	53708.07	158.70
6b	3810.35	53479.90	159.50
7	2890.51	54399.74	371.80
8	2351.89	54938.36	376.50
9	1791.86	55498.39	313.60
10	86.95	57290.25	325.60
11	217.55	57290.25 ± 217.15	77.90
12a	274.70	57290.25 ± 274.70	35.00
12b	369.65	57290.25 ± 369.65	35.50
13a	300.45	57290.25 ± 300.45	15.50
13b	344.10	57290.25 ± 344.10	15.80
14a	312.24	57290.25 ± 312.24	7.93
14b	332.19	57290.25 ± 332.19	7.81
15a	317.60	57290.25 ± 317.60	2.93
15b	321.70	57290.25 ± 321.70	13.00
16	5456.72	88240.74	1970.00
17	922.60	165515.92	2981.60
18	7013.21	183252.23 ± 7013.21	1948.00

Channel	*IF Center Frequency (MHz)*	*RF Center Frequency (MHz)*	*RF Bandwidth (MHz)*
19	4487.91	183252.23 ± 4487.91	1899.00
20	2994.30	183252.23 ± 2994.30	988.20
21	1790.50	183252.23 ± 1790.50	981.80
22	1000.75	183252.23 ± 1000.75	507.30

9.2 Spectral Response Functions Characteristics

The ATMS Spectral Response Function (SRF) in Figure 9-1 is defined by a one-to-one mapping between actual measured end-to-end gain values to the RF frequencies of radiation relevant to each channel, ideally from the antenna aperture through the detector output. For a channel having multiple pass bands, the SRF of each passband is unique and not affected by the SRF of other passbands of the same channel. In practice, the SRFs were solely based on the measured receiver SRFs and do not include contributions from the flight antenna.

The ATMS SRFs are used to generate: 1) Band absorption coefficients for radiative transfer models used by environmental retrievals algorithms and Numerical Weather Prediction (NWP) models. NWP models continue to require more accurate SRF measurements. 2) Band conversion coefficients in the operational SDR algorithm that calculate warm/cold target radiance from their physical temperatures and Earth spectral brightness temperature from Earth radiance.

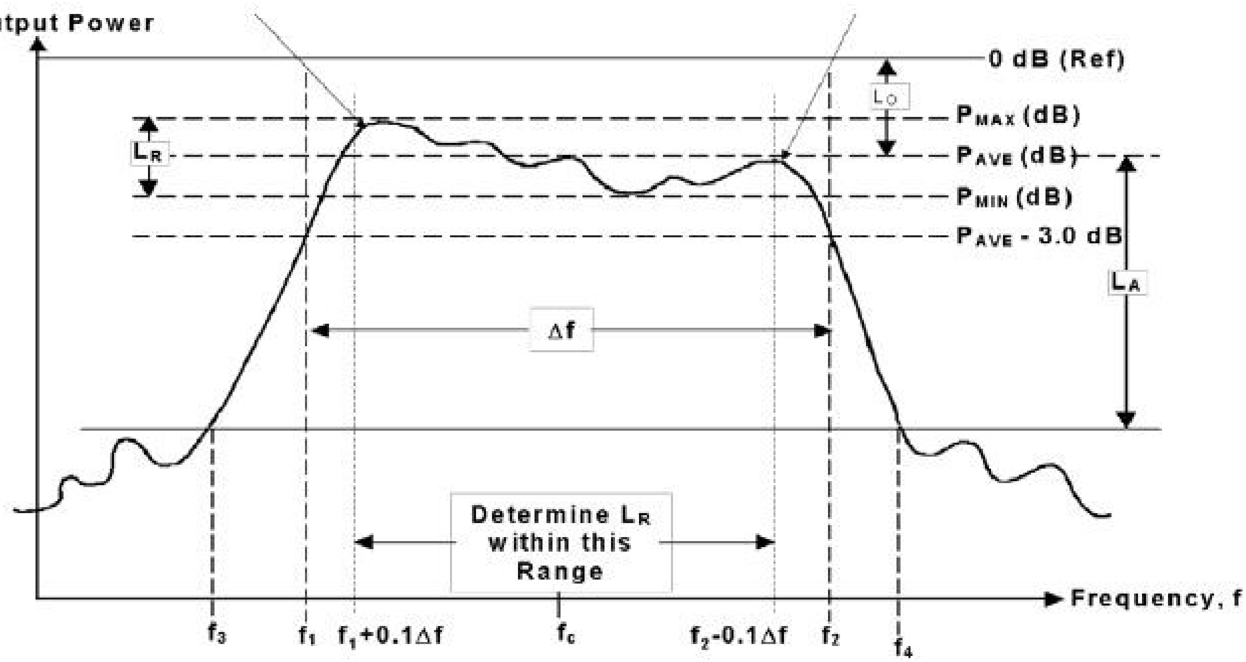

Figure 9-1: Demonstrations of how to measure the SRF versus Frequency

In Figure 9-1,

P_{MAX} : max power ($f_{roll\ off\ low}$ to $f_{roll\ off\ high}$)
P_{MIN} : min power ($f_{roll\ off\ low}$ to $f_{roll\ off\ high}$)
P_{AVE} : $(P_{MAX} + P_{MIN})/2$
L_0 : passband insertion loss (dB)

L_A	: out-of-band rejection (dB)
Passband	: f_1 to f_2
Stopband	: $f < f_3$ and $f > f_4$
f_{CENTER}	: $(f_1 + f_2)/2$
Bandwidth	: $\Delta f = f_2 - f_1$
L_R	: passband ripple

The QS ATMS SRF data can be found in Appendix F.

For each of the four channel groupings in the 22 channels of ATMS, the data consists of the processed data from raw data measured by the instrument contractor. The four channels' groupings are channels 1 and 2 (direct detect), 3-15 which consists of 3-9 (single sideband) and 10-15 (double sideband), 16 (single sideband), 17-22 (double sideband). Note that Channel 6 has two passbands in the lower sideband, with respect to the Local Oscillator (LO) frequency. There are four passbands for channels 12-15.

All the provided QS SRF data are stored in .csv file format.

10. RADIOMETRIC COUNTS DYNAMIC RANGE

The ATMS end-to-end system gain is expected to vary by no more than ± 2 dB over the life of the instrument. Thus, for a 16-bit A-to-D conversion, the radiometric count maximum, Cmax = 65535 – 2 dB = 65535 – 10192*2 = 45151, which is the expected minimum count of "upper guard band" for all ATMS 22 channels. Adding a video offset voltage to adjust counts is not implemented on ATMS, so the counts are determined and approximated from the channel gain (Counts/K) and noise figure, i.e., Tsys, the system noise temperature, see next section.

Figure 10-1 below shows also a "lower guard band" that establishes the value of Cmin = 10192. The intention for specifying such a guard band is for the case where a negative offset voltage is applied to the video output to increase the gain without exceeding the Cmax limit. In that situation, the guard band provides margin against the application of excessive negative offset. For the ATMS design, however, there is adequate gain without applying any video offset. The resulting minimum count, without video offset, is 10,008. If the design were modified to meet the Cmin = 10,192 constraint, the gain would need to be decreased, and a positive offset voltage applied to the video output. The consequence of this would be increased quantization noise and degraded performance. Shown below in Figure 10-1 is QS ATMS dynamic count ranges of all 22 ATMS channels for the nominal gain, as well as nominal gain +/- 2 dB, compared to QS TVAC measured counts at 3K and 330K, respectively. Note that the measured counts are comparable to the predicted counts.

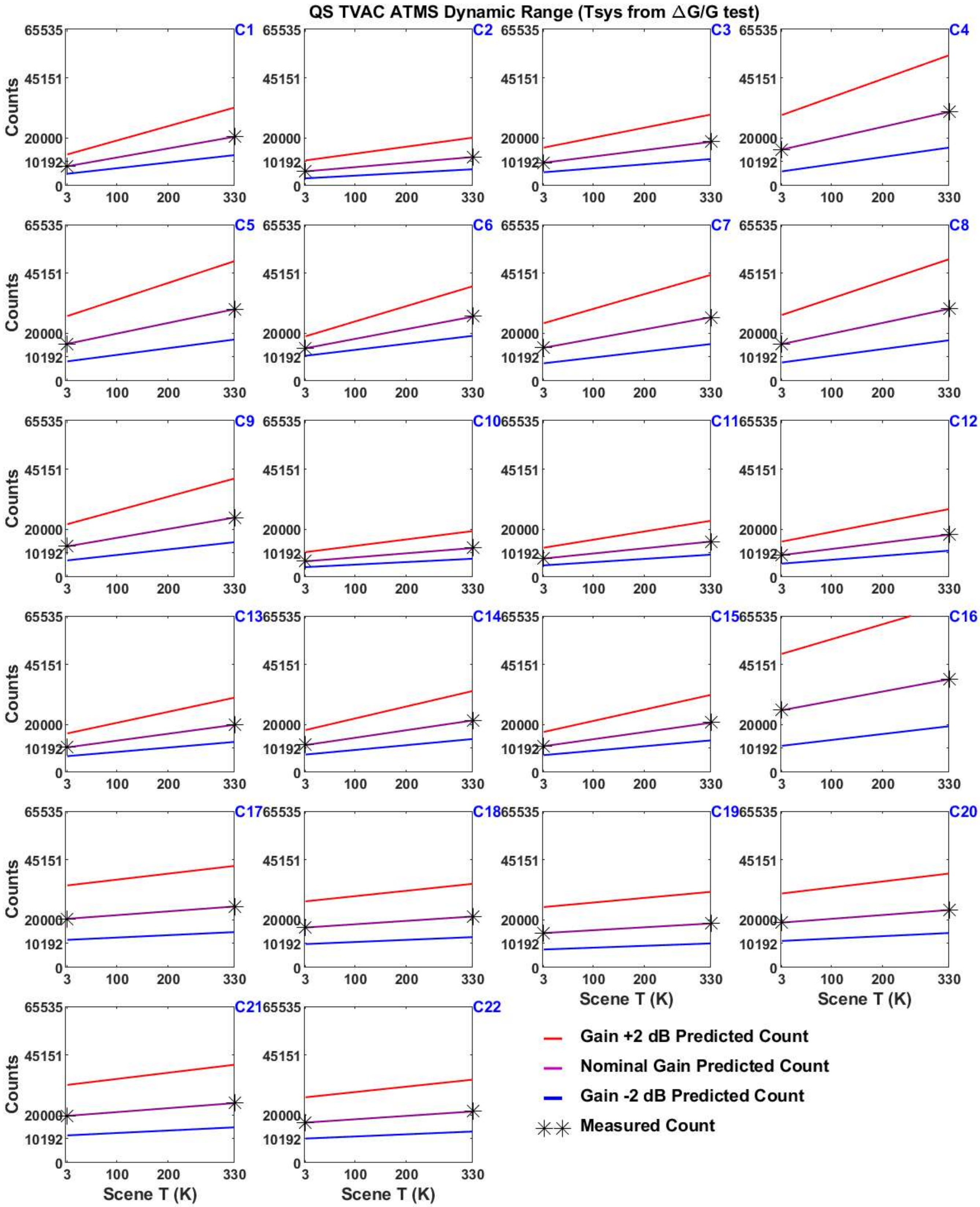

Figure 10-1: QS ATMS 16 bits A/D converter dynamic range, model prediction versus measured TVAC counts.

Note Channel 16 exceeds the upper bound with +2dB gain, but this does not impact Channel 16 performance. Channels 17 - 22 dynamic ranges are ~ 4000 - 5000 counts. QS on-orbit dynamic ranges are about the same as that model predicted from the ground TVAC test.

The dominant temperature on Tsys is the scene target temperature, Tscene. For the dynamic range we calculate Tsys for a 3K and 330K scene and for NEDT compliance shown in Table 8.1, which we use a Tscene of 300K. The secondary contribution on Tsys is Trec. Trec is dominated by receiver noise figure, which tends to be higher at higher hardware temperatures. For the sensor performance study, we use Trec from measured receiver data which tends to be at higher hardware temperatures, and a 300K scene. For the Tsys from the ΔG/G test, see the subsequent section for details.

11. RADIOMETRIC SHORT-TERM GAIN STABILITY

Gain Stability, ΔG/G, data were collected while observing 280K at the mid, low, and high cold plate temperatures for Redundancy Configuration 1. Fast Fourier Transform (FFT)'s was performed on the data, and averaged spectra obtained. There is no specified requirement for ΔG/G values. For ATMS, dG/G is a measure of 1/f noise content, which is the driver behind striping behavior. So although ATMS has no specific requirement on dG/G, we provide values for use in striping-related analyses.

The computations were performed as follows. The total noise equivalent temperature of the power spectrum, *X(j)*, in terms of frequency (Hz) vs. K^2, is taken as the square root of the sum of the unfiltered spectrum data points, excluding the DC point and alias points, as shown.

$$T_{total} = \sqrt{\sum_{j=2}^{n-m} X(j)} \quad \text{Equation 11-1}$$

Where: n=Total points in the spectra, typically 1024

m=Alias backoff, typically 20

The white noise portion is computed as follows.

$$T_{white} = \sqrt{\frac{(n-m-1)}{(n-m-k+1)} * \sum_{j=k}^{n-m} X(j)} \quad \text{Equation 11-2}$$

Where:

k=White noise starting point, typical points and frequencies provided below

	k	f (Hz)
CH01-15	923	25
CH16	923	25
CH17-22	923	25

The delta, representing the temperature "flicker" noise, is calculated as follows.

$$T_{delta} = \sqrt{T_{total}{}^2 - T_{white}{}^2}$$ Equation 11-3

$$T_{sys} = T_{white}\sqrt{BW * 17660}$$ Equation 11-4

where BW = Bandwidth of Corresponding Channel (MHz)

τ = 17660 μsec, which is ATMS one footprint (field of view) integration time

The ΔG/G values in terms of Tsys, from the Ulaby and Long definition, are calculated as follows.

$$\frac{\Delta G}{G}(sys) = \frac{T_{delta}}{T_{sys}}$$ Equation 11-5

The ΔG/G values in terms of T_{total} are calculated as follows.

$$\frac{\Delta G}{G}(tot) = \frac{T_{delta}}{T_{total}}$$ Equation 11-6

Now we can derive NEDT by using the following approach.

$$NEdT = \left[\left(T_{SYS}\frac{\Delta G}{G}(sys)\right)^2 + \left(\frac{T_{SYS}}{\sqrt{B\tau}}\right)^2\right]^{1/2}$$ Equation 11-7

Or

$$NEdT = [(T_{delta})^2 + (T_{White})^2]^{1/2}$$ Equation 11-8

Note to be consistent with the instrument measured NEdT, the total NEdT needs to include calibration error. Note also that the following data are summarized for each of the cold plate (CP) temperatures (+5 °C, +15 °C, +25 °C and +2.5 °C) in Table 11.1- Table 11.4.

Table 11.1: Gain Stability Data (for CP = +5° C, using the best fits), Tscene = 280K

CH	BW (MHZ)	TSYS (K)	TTOTAL (K)	TWHITE (K)	TDELTA (K)	ΔG/G (TOT)	NEDT (K)
1	265.9	486.8	0.239	0.220	0.095	0.363	0.24
2	171.6	680.7	0.474	0.367	0.300	0.573	0.49
3	163.9	647.6	0.479	0.354	0.324	0.612	0.44
4	395.9	741.7	0.393	0.252	0.302	0.703	0.36
5	384.2	697.9	0.365	0.244	0.272	0.682	0.34
6	320.6	472.4	0.368	0.265	0.256	0.649	0.36
7	383.8	700.2	0.362	0.247	0.264	0.670	0.35
8	380.3	704.1	0.366	0.250	0.268	0.673	0.36
9	310	673.8	0.371	0.269	0.255	0.634	0.36
10	151.9	642.1	0.453	0.376	0.253	0.507	0.45
11	76.7	614.4	0.572	0.517	0.246	0.400	0.55
12	69.8	626.4	0.605	0.552	0.247	0.378	0.59
13	31	604	0.842	0.804	0.248	0.272	0.82
14	15.8	600.7	1.150	1.124	0.239	0.198	1.18
15	5.8	596.8	1.862	1.846	0.248	0.120	1.86
16	1934.6	1225.8	0.448	0.205	0.399	0.874	0.44
17	1121.5	1737.9	0.580	0.367	0.449	0.740	0.5
18	1942.8	1566.9	0.338	0.250	0.228	0.616	0.36

CH	BW (MHZ)	TSYS (K)	TTOTAL (K)	TWHITE (K)	TDELTA (K)	ΔG/G (TOT)	NEDT (K)
19	1903.8	1780.2	0.386	0.285	0.261	0.610	0.41
20	978.6	1531	0.416	0.350	0.224	0.477	0.42
21	976	1581.6	0.455	0.357	0.283	0.557	0.46
22	490.7	1515.9	0.582	0.497	0.302	0.478	0.58

Table 11.2: Gain Stability Data (for CP = +15° C, using the best fits), Tscene = 280K

CH	BW (MHZ)	TSYS (K)	TTOTAL (K)	TWHITE (K)	TDELTA (K)	ΔG/G (TOT)	NEDT (K)
1	265.9	501.3	0.250	0.226	0.107	0.394	0.25
2	171.6	705.4	0.506	0.379	0.334	0.605	0.54
3	163.9	680.8	0.516	0.366	0.364	0.638	0.48
4	395.9	789.8	0.427	0.259	0.339	0.718	0.39
5	384.2	725.3	0.377	0.251	0.281	0.678	0.37
6	320.6	488.5	0.380	0.267	0.270	0.648	0.38
7	383.8	727.7	0.373	0.254	0.274	0.666	0.39
8	380.3	740.4	0.385	0.259	0.285	0.673	0.4
9	310	707.8	0.398	0.276	0.288	0.654	0.41
10	151.9	664.7	0.470	0.385	0.270	0.515	0.5
11	76.7	633	0.592	0.531	0.262	0.413	0.62
12	69.8	645.9	0.627	0.566	0.270	0.392	0.66
13	31	622.8	0.872	0.838	0.240	0.291	0.9
14	15.8	618.6	1.183	1.166	0.199	0.203	1.2
15	5.8	616.9	1.925	1.910	0.236	0.124	1.91
16	1934.6	1295.1	0.503	0.219	0.453	0.883	0.5
17	1121.5	1795.2	0.596	0.375	0.462	0.736	0.61
18	1942.8	1602.5	0.335	0.260	0.211	0.581	0.32
19	1903.8	1792.7	0.379	0.288	0.246	0.582	0.37
20	978.6	1570.1	0.424	0.363	0.220	0.469	0.42
21	976	1634.7	0.469	0.373	0.283	0.550	0.47
22	490.7	1548.9	0.596	0.508	0.311	0.479	0.59

Table 11.3: Gain Stability Data (for CP = +25° C, using the best fits), Tscene = 280K

CH	BW (MHZ)	TSYS (K)	TTOTAL (K)	TWHITE (K)	TDELTA (K)	ΔG/G (TOT)	NEDT (K)
1	265.9	517	0.267	0.232	0.132	0.461	0.27
2	171.6	727.7	0.537	0.391	0.368	0.630	0.51
3	163.9	678.9	0.523	0.372	0.368	0.649	0.49
4	395.9	776.4	0.430	0.264	0.339	0.731	0.41
5	384.2	732	0.391	0.256	0.296	0.697	0.36
6	320.6	500.7	0.402	0.271	0.296	0.673	0.37
7	383.8	748.9	0.404	0.260	0.309	0.703	0.37
8	380.3	756.6	0.418	0.262	0.326	0.717	0.38
9	310	726.6	0.435	0.285	0.328	0.700	0.39
10	151.9	690.3	0.500	0.404	0.294	0.542	0.49

CH	BW (MHZ)	TSYS (K)	TTOTAL (K)	TWHITE (K)	TDELTA (K)	ΔG/G (TOT)	NEDT (K)
11	76.7	656.8	0.625	0.548	0.302	0.440	0.62
12	69.8	669.6	0.661	0.583	0.311	0.422	0.65
13	31	648.6	0.914	0.860	0.307	0.307	0.93
14	15.8	642.9	1.237	1.198	0.310	0.222	1.24
15	5.8	636.1	1.988	1.959	0.343	0.134	2
16	1934.6	1391.1	0.552	0.235	0.499	0.888	0.51
17	1121.5	1845.1	0.624	0.386	0.489	0.747	0.59
18	1942.8	1631.6	0.323	0.267	0.181	0.507	0.32
19	1903.8	1784.1	0.367	0.289	0.226	0.543	0.37
20	978.6	1602.5	0.435	0.369	0.230	0.475	0.46
21	976	1680.2	0.484	0.385	0.292	0.553	0.5
22	490.7	1584.5	0.616	0.518	0.333	0.492	0.62

Table 11.4: Gain Stability Data (for QS On-orbit, CP=2.50K, using the best fits), Tscene@ICT (ICT KaV=278.56K & ICT WG=279.44K, to be updated post-launch)

CH	BW (MHZ)	TSYS (K)	TTOTAL (K)	TWHITE (K)	TDELTA (K)	ΔG/G (TOT)	NEDT (K)
1	265.69	462.468	0.219	0.214	0.047	0.216	0.219
2	170.12	468.163	0.275	0.270	0.049	0.179	0.275
3	178.20	532.446	0.306	0.300	0.062	0.202	0.306
4	376.42	519.649	0.211	0.202	0.062	0.293	0.211
5	388.50	513.152	0.205	0.196	0.060	0.292	0.205
6	322.92	502.601	0.219	0.210	0.061	0.280	0.219
7	387.00	516.459	0.207	0.198	0.061	0.294	0.207
8	373.50	516.889	0.211	0.201	0.062	0.296	0.211
9	315.75	513.493	0.226	0.217	0.061	0.272	0.226
10	152.16	541.613	0.336	0.330	0.059	0.176	0.336
11	77.98	528.269	0.454	0.450	0.057	0.126	0.454
12	69.35	545.691	0.497	0.493	0.061	0.123	0.497
13	30.84	521.927	0.710	0.707	0.063	0.089	0.710
14	15.72	523.230	0.995	0.993	0.068	0.069	0.995
15	5.82	524.104	1.635	1.635	0.048	0.030	1.635
16	1938.52	908.677	0.204	0.155	0.133	0.650	0.204
17	1146.30	1403.21	0.318	0.312	0.060	0.189	0.318
18	1939.19	1484.958	0.255	0.254	0.024	0.094	0.255
19	1962.13	1532.792	0.261	0.260	0.021	0.082	0.261
20	961.09	1487.284	0.363	0.361	0.036	0.099	0.363
21	979.51	1514.700	0.367	0.364	0.044	0.119	0.367
22	489.70	1468.343	0.500	0.499	0.029	0.057	0.500

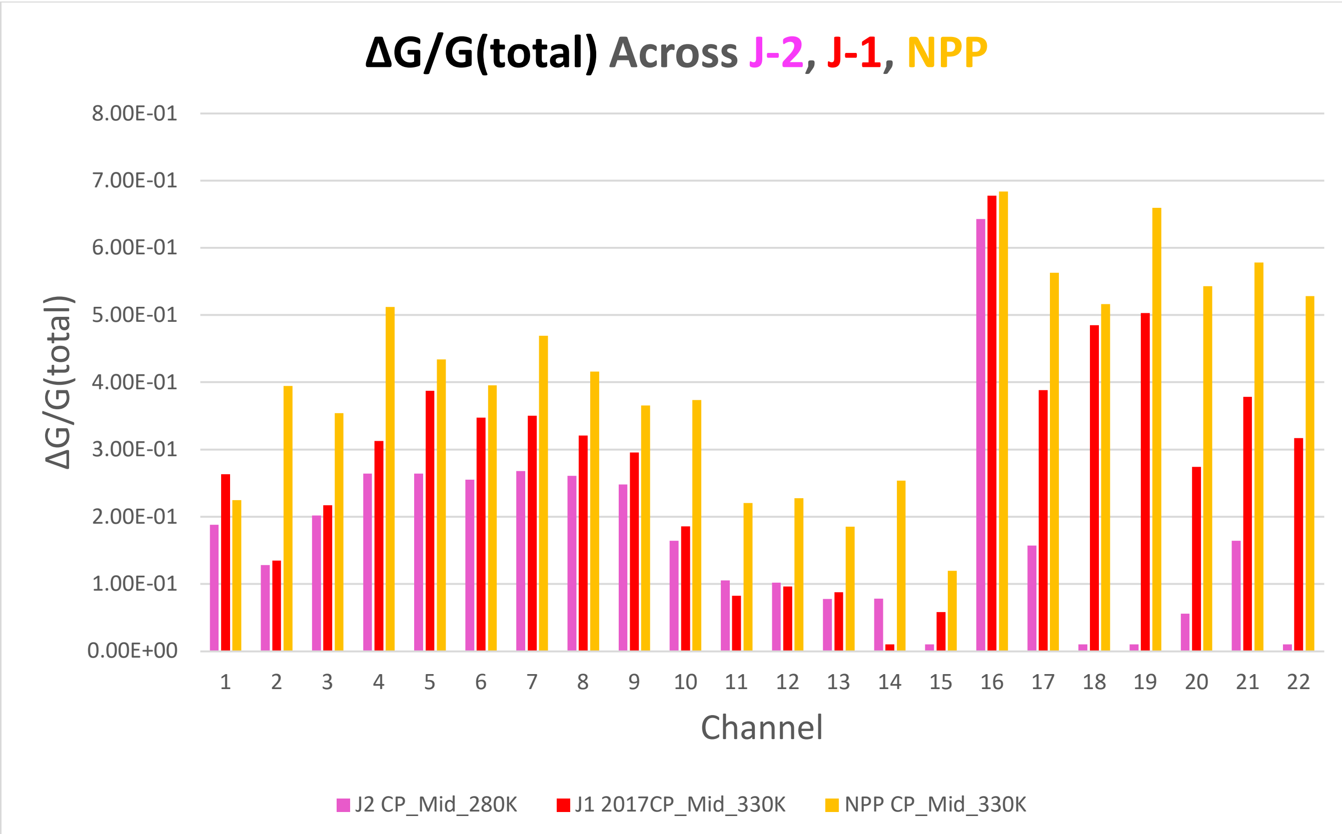

Figure 11-1: QS ATMS ΔG/G(total) metric of 1/f content (to be updated post-launch).

From the ATMS short term gain stability ΔG/G tests, one can use ΔG/G(total) as another gauge of ATMS striping performance. Comparing QS to previous JPSS ATMS builds JPSS-2, JPSS-1 and SNPP, one can find significantly reduced striping noise in the J2 ATMS data, see Figure 11-1. QS shows slightly larger striping noise than NPP. This is because the smaller ΔG/G(total) is, the less striping will be found in the ATMS data.

12. STRIPING INDEX

The striping effect can be observed in the pre-launch instrument level thermal vacuum (TVac) test data. One good example is Shown in Figure 12-1. It demonstrates the brightness temperature bias between the linear calibrated scene target temperatures, from the QS and JPSS-2 ATMS RC1 TVac data, respectively, and the corresponding measured scene target (PRT) temperatures at 300 K scene for ATMS FOVs 13 to 18 of all channels. Compared to the JPSS brightness temperature bias, QS brightness temperature bias presented more significant along-track striping feature. This striping effect also demonstrates a channel dependent character.

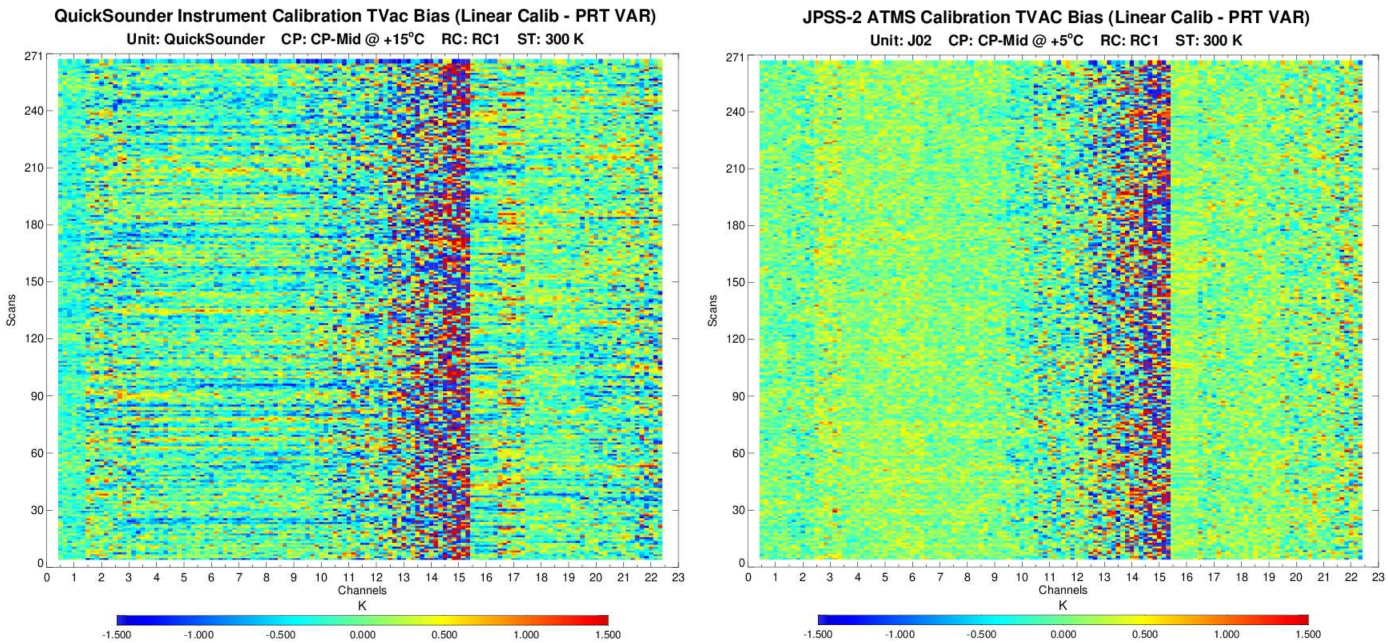

Figure 12-1: QS (left) and JPSS-2 (right) ATMS instrument calibration TVAC RC1 brightness temperature bias between linear calibrated and measured scene target at 300K

The striping effect can also be found in Suomi NPP on-orbit radiance data when the data are subtracted by the Radiative Transfer Model (RTM) simulation using numerical weather prediction (NWP) system output profiles [5] during the post-launch data quality evaluation. The noise contributed by striping effects may also cause the increase of channel correlation. Illustrated in Figure 12-2 are the O-B (differences between satellite Observations and RTM simulations) biases for S-NPP and NOAA-21 ATMS channel 9, derived by using SDR subtracted from Community RTM (CRTM) simulation, with respect to ECMWF forecast data. On August 20, 2024, the S-NPP O-B difference demonstrates relatively higher striping effects compared to NOAA-21. (To be updated with QS on-orbit O-B after launch to replace S-NPP).

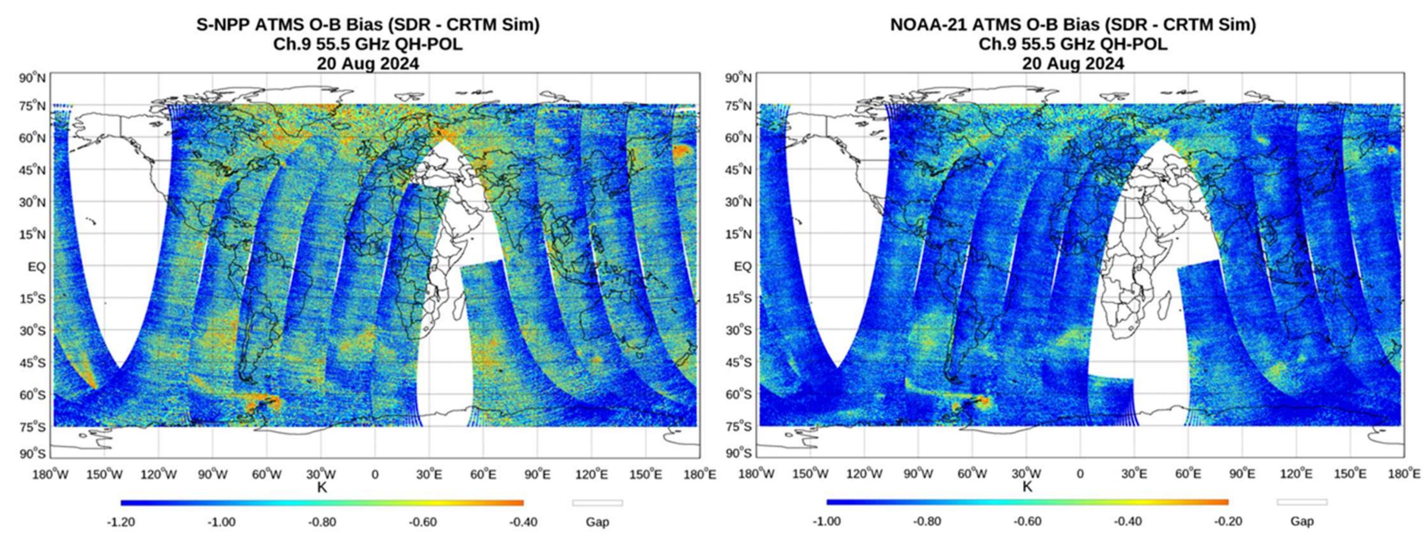

Figure 12-2: S-NPP & QS ATMS channel 9 on-orbit SDR vs. CRTM simulation bias on Aug. 20, 2024.

Compared to QS, similar striping was found in S-NPP data. (To be updated using QS on-orbit data)

To evaluate the striping effect, QS ATMS Cal/Val team uses Striping Index (SI) to indicate the scale of striping effect. SI is defined as the ratio of down-track variance to cross-track variance of the observed brightness temperatures.

$$SI = V_{DT} / V_{CT} \quad \text{Equation 12-1}$$

In the equation above, the definition of V_{CT} and V_{DT} are,

$$V_{CT} = \frac{1}{N_{SCAN}} \sum_{j=1}^{N_{SCAN}} V_1(j) \quad \text{Equation 12-2}$$

$$V_1(j) = \frac{1}{N_{FOV}} \sum_{i=1}^{N_{FOV}} [T_B(i,j) - \overline{T}_B(j)]^2, \qquad \overline{T}_B(j) = \frac{1}{N_{FOV}} \sum_{i=1}^{N_{FOV}} T_B(i,j) \quad \text{Equation 12-3}$$

and,

$$V_{DT} = \frac{1}{N_{FOV}} \sum_{i=1}^{N_{FOV}} V_2(i) \quad \text{Equation 12-4}$$

$$V_2(i) = \frac{1}{N_{SCAN}} \sum_{j=1}^{N_{SCAN}} [T_B(i,j) - \overline{T}_B(i)]^2, \qquad \overline{T}_B(i) = \frac{1}{N_{SCAN}} \sum_{j=1}^{N_{SCAN}} T_B(i,j) \quad \text{Equation 12-5}$$

If SI is significantly larger than 1, it indicates a down-track scan-to-scan variability (striping).

SI can be computed using pre-launch instrument level thermal vacuum (TVAC) data in order to verify sensor hardware performance. List in Table 12.1 is the S-NPP, JPSS-2, JPSS-1, and QS channel dependent SI calculated from instrument TVAC CP-Mid (Cold Plate at Mid temperature) data. For QS ATMS SI calculation using TVAC data, NFOV=6 (FOV 14 to 19) and NSCAN=10 (5 scans before and 4 scans after the current scan) are used in calculation.

Table 12.1: S-NPP, JPSS-2, JPSS-1, and QS ATMS Instrument TVAC CP-Mid Striping Index

CHANNEL	CENTER FREQUENCY (MHZ)	S-NPP SI CP +5 C	JPSS-1 SI CP +7.7 C	JPSS-2 SI CP +5 C	QS SI CP +15 C
1	23800	1.060	1.065	1.052	1.167
2	31400	1.191	1.036	1.035	1.503
3	50300	1.148	1.054	1.056	1.610
4	51760	1.259	1.099	1.084	1.950
5	52800	1.280	1.160	1.073	1.768
6	53596±115	1.223	1.124	1.068	1.650
7	54400	1.252	1.132	1.078	1.714
8	54940	1.234	1.117	1.082	1.732
9	55500	1.161	1.103	1.065	1.656
10	57290.344(f_o)	1.151	1.043	1.040	1.332
11	f_o± 217	1.093	1.033	1.027	1.202

CHANNEL	CENTER FREQUENCY (MHZ)	S-NPP SI CP +5 C	JPSS-1 SI CP +7.7 C	JPSS-2 SI CP +5 C	QS SI CP +15 C
12	f_o±322.2±48	1.088	1.024	1.026	1.176
13	f_o±322.2±22	1.049	1.022	1.021	1.093
14	f_o±322.2±10	1.039	1.016	1.024	1.050
15	f_o±322.2±4.5	1.024	1.020	1.016	1.032
16	88200	1.707	1.619	1.535	2.948
17	165500	1.639	1.143	1.045	1.967
18	183310±7000	1.346	1.287	1.015	1.507
19	183310±4500	1.618	1.314	1.020	1.501
20	183310±3000	1.405	1.103	1.020	1.266
21	183310±1800	1.603	1.191	1.042	1.384
22	183310±1000	1.510	1.130	1.021	1.263

Shown in Figure 12-3 is the SI comparison chart based on the data in Table 12.1. It is found that the striping effect of S-NPP, JPSS-1 and JPSS-2 has been reduced compared to QS. QS channels demonstrate mostly worst or significant SI than S-NPP.

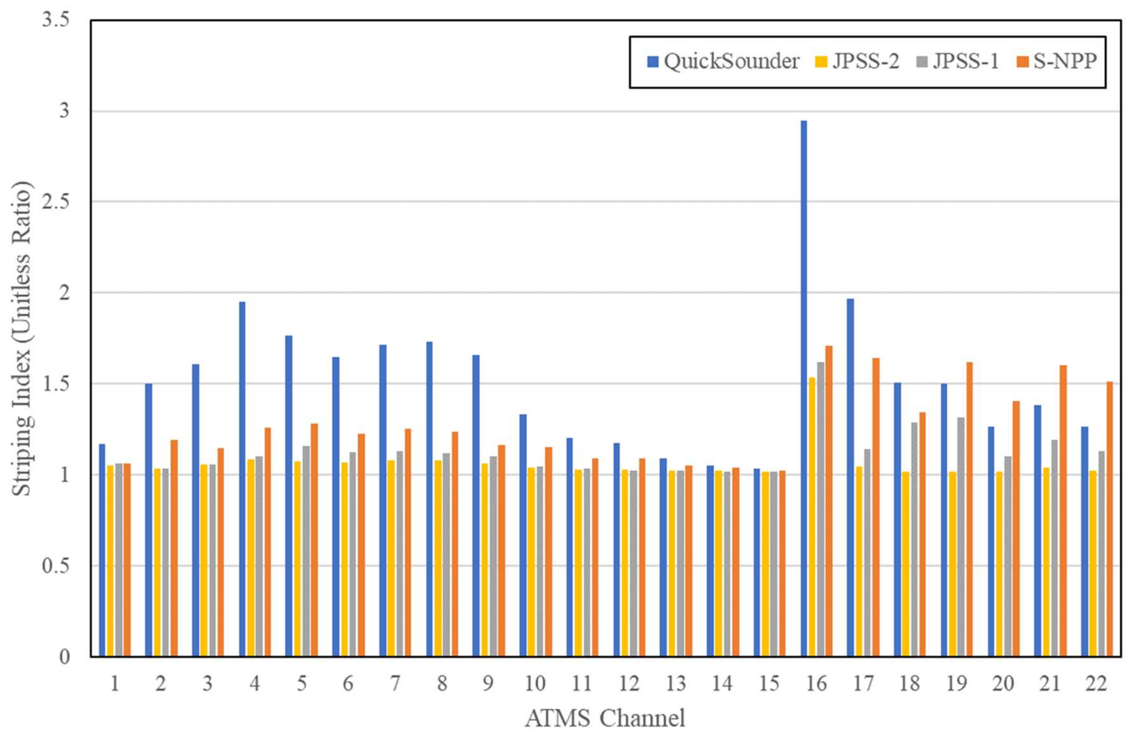

Figure 12-3: QuickSounder (QS), JPSS-2, JPSS-1, and S-NPP ATMS instrument TVAC CP-Mid SI comparison

The on-orbit SI can only be assessed using the observations (SDR) minus RTM simulation data, as shown in Figure 12-3. However, due to the surface emissivity impact in near surface channels and water vapor distribution impact in G-band channels radiative transfer simulations, the on-orbit SI analysis results are more reliable at channel 6 to 15. Displayed in Figure 12-4 are the SI comparisons of three on-orbit ATMS instruments for the reference. For QS ATMS on-orbit SI calculation using observation minus simulation data, NFOV=10 (FOV 44 to 53) and NSCAN=10 (5 scans before and 4 scans after the current scan) are used in calculation. The on-orbit SI values of displayed channels are slightly different from what are calculated from TVAC data, shown above. However, the relative difference pattern among the three instruments is very similar to those of TVAC results.

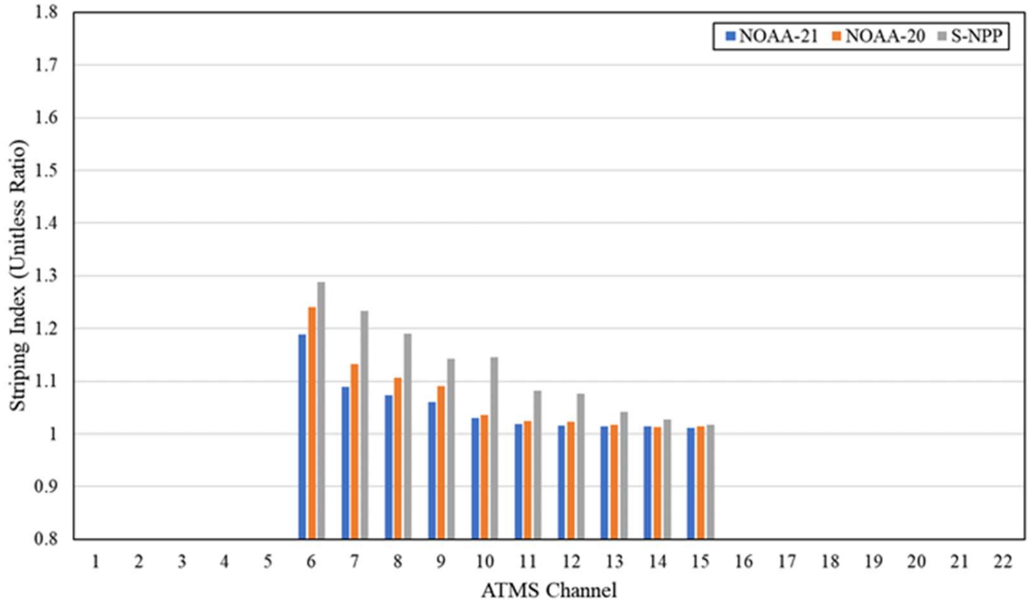

Figure 12-4: QS, NOAA-20, and S-NPP ATMS channel 6 to 15 SI comparison based on the on-orbit data on August 7, 2024 (To be updated)

13. ON-ORBIT PROCESSING PCT TABLES

The implementation and improvement of calibration results are applied to raw observations through Processing Coefficients Table (PCT) in the operational Interface Data Processing Segment (IDPS) in order to generate user friendly brightness temperature. The PCT is binary data including both satellite dependent and independent coefficients derived from both pre-launch TVAC and Post-Launch Test (PLT) on-orbit data analysis results. Due to the difference in primary and redundant spectral response function (SRF) data, the central frequency and radiance band correction coefficients are different in Side-A and Side-B PCT files, respectively. Before applying for PCT for ATMS calibrations, one needs to know ATMS Radiometric Counts Limits, in Table 13.1. List in Table 13.2 is the coefficient names and brief descriptions in current PCT.

Table 13.1: ATMS Radiometric Counts Limits (To be updated post-launch)

Channel	Minimum for Ts=3 K Target	Maximum for Ts=330 K Target
1	8150	20538
2	6005	12016
3	9634	18394
4	15149	30943
5	15556	30078
6	13840	27065

Channel	Minimum for Ts=3 K Target	Maximum for Ts=330 K Target
7	13909	26685
8	15463	30196
9	12851	24923
10	6618	12177
11	7763	14884
12	9197	17790
13	10535	19987
14	11501	21819
15	11039	20841
16	26014	38991
17	20426	25578
18	16757	21389
19	14441	18463
20	18839	24110
21	19659	24999
22	16842	21504

Table 13.2: ATMS IDPS PCT Contents

Parameter	Description	Ref. Note
scanWeightsWc	Warm count calibration window scan weight	Boxcar 10 scans except channel 17, 21, and 22, which use 5 scans
scanWeightsCc	Spaceview count calibration window scan weight	Same as above
scanBias	Angular dependent bias correction	See section 5.4
beamEfficiencyCorrection	Beam efficiency correction	See section 5.4
warmBiasCorrection	Warm load (WL) PRT bias correction	See section 8.4.1
instr2scMatrix	Mounting matrix	Set it to an Identity Matrix, using Table 5.2 only*
centralFrequency	Primary (A) & Redundant (B) Channel central frequency for Planck function	See section 9.1
radianceBandCorrection	Primary & Redundant Frequency dependent temperature correction coefficients for Planck function	See section 9.1
lunarIntrusionCorrectionOmiga	Lunar intrusion correction coefficients	See section 7.2
lunarIntrusionCorrectionAlpha	Lunar intrusion correction coefficients	See section 7.2
lunarIntrusionCorrectionSigma	Lunar intrusion correction coefficients	See section 7.2
lunarIntrusionCorrectionMoonEmissivity	Lunar intrusion correction moon emissivity	See section 7.2

Parameter	Description	Ref. Note
scanWeightsPrtKav	KAV PRT reading weight	Boxcar for all 8 readings of K/Ka/V-band
scanWeightsPrtWg	WG PRT reading weight	Boxcar for all 7 readings of W/G band
coldSpaceTbs	RJ based Spaceview brightness temperature	Not used in full radiance calibration
quadraticRc	Radiance based non-linearity correction coefficients	See section 8.3
shelfTemp	Shelf temperature used for RJ based quadratic coefficient interpolation	Not used in full radiance calibration
beamAlignmentError	Beam alignment correction coefficients	See section 5.2
coldBiasCorrection	Spaceview temperature correction coefficients	See section 8.4.2
lowLimitPrt	WL PRT temperature lower limit	245 K for K/Ka/V and W/G bands
uppLimitPrt	WL PRT temperature upper limit	340 K for K/Ka/V and W/G bands
maxVarPrt	Allowed PRT reading variance limit	5 K for K/Ka/V and W/G bands
threeDBeamWidth	3 dB beam width	See section 5.1
lunarContaminationThreshold	Lunar intrusion threshold	0.2 K
prtConvergence	PRT calculation residual	0.001 K
wtThresholdPrt	All good PRT weight	0.7 (70%)
wtThresholdWc	All good warm count weight	0.7 (70%)
wtThresholdCc	All good spaceview count weight	0.7 (70%)
dataLimits	Instrument telemetry health status limits	See section 3.5
reflectorEmissivity	Reflector emissivity	See section 5.3
reflectorTempOffset	Reflector temperature offset	0 (for reflector temperature adjustment)
spaceViewresolverCounts	Spaceview reading resolver count	See Table 4.2
blackBodyResolverCounts	Warm load reading resolver count	See Table 4.2
lowLimitWc	Warm count lower limit	See Table 13.1
uppLimitWc	Warm count upper limit	See Table 13.1
maxVarWc	Allowed warm count variance limit	Channel dependent fixed values for all builds
lowLimitCc	Spaceview count lower limit	See Table 13.1
uppLimitCc	Spaceview count upper limit	See Table 13.1
maxVarCc	Allowed spaceview count variance limit	Same as maxVarWc
numThresholdPrt	Number of good PRT readings per scan	5 for K/Ka/V band 4 for W/G band
mapRc	RC numbers	[1,4,2,3]
resolverOffset	Resolver offset	Measured value 0 counts

Parameter	Description	Ref. Note
epsilonCold	QC - Allowed SV resolver count variance limit	70
epsilonWarm	QC - Allowed WC resolver count variance limit	70
allowableDev	QC - Time sequence error limit	19 msec
prtLoops	QC - PRT calculation max number of loops	100
useQuadraticTerm	Flag - Use quadratic correction coefficients in PCT flag	1
useQuadraticTele	Flag - Use quadratic correction coefficients in calibration packet flag	0
useBeamAlignTele	Flag - Use beam alignment error correction coefficients in calibration packet flag	0
useWarmBiasTele	Flag - Use warm bias correction coefficients in calibration packet flag	0
useColdBiasTele	Flag - Use cold bias correction coefficients in calibration packet flag	0
chkConsistWcCc	Flag - Check Warm Count/Cold Count consistency flag	1
chkConsistPrt	Flag - Check PRT consistency flag	1

*Setting the instr2scMatrix to an identity matrix, because Instrument to s/c mounting coefficients are already used in deriving the Euler angles for QS ATMS antenna beam pointing offset in Satellite Coordinates, presented in Table 5.2

Note that lowLimitWc=lowLimitCc and uppLimitWc=uppLimitCc;

14. INTRODUCING NOAA ICVS WEBSITE AND SERVICES

NOAA STAR's Integrated Calibration/Validation System (ICVS) website provides near-real-time environmental satellite performance and scientific data quality monitoring. The ICVS Long-Term Monitoring (LTM), ICVS-LTM, System allows visualization and comparison of data related to satellite instruments from Suomi National Polar Orbiting Partnership (SNPP), the JPSS missions, NOAA legacy Polar Operational Environmental Satellites (POES), Geostationary Operational Environmental Satellites (GOES), and the QuickSounder (QS) mission. For convenience, the ICVS website link is https://www.star.nesdis.noaa.gov/icvs/index.php .

For each of the missions, data are organized per instrument supporting the monitoring of the time variations of key parameters, for instance science parameters (NEDT, gain, counts…), telemetry parameters (shelf temperatures, instrument temperatures, instrument health) or quality flags in the case of ATMS. The health and status of QS ATMS can be monitored throughout the mission by looking at the variations of the shelf temperatures, for instance, or the variations of NEDT.

Another important feature of ICVS is to provide inter-satellite comparison of radiances. One method is to use the observation minus radiative transfer model simulation (O-B) bias to determine double bias difference results to indicate the observational bias between two ATMS instruments. Another way to estimate the inter-sensor bias is to calculate the 32-day observation running mean to derive direct bias. Both methods allow assessment of the calibration of QS ATMS, compared to ATMS from other satellites like NOAA-21 and NOAA-20. There is no regular Simultaneous Nadir Overpass (SNO) among JPSS missions for inter-sensor bias comparison.

NOAA also developed the Comprehensive Large Array-data Stewardship System (CLASS) which stores all JPSS ATMS data products for all JPSS missions. Therefore, the QS ATMS Raw Data Record (RDR), Temperature Data Record (TDR), Sensor Data Record (SDR) and ATMS Environmental Data Records (EDRs) products are available for download from the CLASS website. The selection of the data can be refined by geographic areas (only a small portion of the world can be selected by providing a latitude/longitude box) and/or time series (by selecting a starting and ending day/time). Note QS data may be available only from NCCF NODD (TBD).

The Center for Satellite Applications and Research (STAR) JPSS website is another resource that hosts ATMS documentation (ATMS Doc), such as the ATMS SDR calibration Algorithm Theoretical Basis Document (ATBD). The ATMS instrument characteristics are described on the QS ATMS instrument page (QS ATMS, To be updated), which also includes downloads for ATMS Spectral Response Functions.

The QS ATMS user guide (user guide) is hosted on the NOAA Institutional Repository. This document describes the operational ATMS science data products such as the antenna temperature data record (TDR), the sensor data record (SDR) and the geolocation. Information about the processing of the data and the generation of these products is also detailed in the user guide.

15. REFERENCE

[1] Yang, H., Weng, F. and Anderson, K., 2016. "Estimation of ATMS antenna emission from cold space observations". IEEE Transactions on Geoscience and Remote Sensing, 54(8), pp.4479-4487.

[2] H. Yang *et al*., "ATMS Radiance Data Products' Calibration and Evaluation," in *IEEE Transactions on Geoscience and Remote Sensing*, vol. 60, pp. 1-11, 2022, Art no. 5302211, doi: 10.1109/TGRS.2021.3123576.

[3] H. Yang et. al., " Developing Vicarious Calibration for MicrowaveSounding Instruments Using Lunar Radiation", *IEEE TRANSACTIONS ON GEOSCIENCE AND REMOTE SENSING*, VOL. 56, NO. 11, pp. 6723-6733, NOVEMBER 2018.

[4] Joint Polar Satellite System (JPSS) Advanced Technology Microwave Sounder (ATMS) SDR Calibration Algorithm Theoretical Basis Document (ATBD)

[5] N. Bormann, A. Fouilloux, and W. Bell, "Evaluation and assimilation of ATMS data in the ECMWF system," *Journal of Geophysical Research: Atmospheres,* vol. 118, no. 23, pp. 12,970-12,980, 2013.

NOTES: ABBREVIATIONS, ACRONYMS, AND SYMBOLS

A/D	Analog/Digital
APC	Antenna Pattern Correction (Coefficients)
APID	Application Identifier
ATMS	Advanced Technology Microwave Sounder
C	Celsius
CH	Channel
dB	Decibel
DB	Direct Broadcast
dBm	Decibel (referenced to one milliwatt)
ECMWF	European Centre for Medium-Range Weather Forecasts
EDU	Engineering Development Unit
EEPROM	Electrically Erasable Programmable Read-Only Memory
FOR	Fields of Regard
FOV	Fields of View
GSFC	Goddard Space Flight Center
GHz	Gigahertz
ICT	Internal Calibration Target
IDPS	Interface Data Processing Segment
IF	Intermediate Frequency
JPSS	Joint Polar Satellite System
K	Kelvin
kHz	Kilohertz
km	Kilometer
LEO&A	Launch, Early Orbit & Activation
LSW	Least Significant Word
MHz	Megahertz
MSW	Most Significant Word
NASA	National Aeronautics and Space Administration
NEDT	Noise Equivalent Delta Temperature
NEON	Near Earth Orbit Network

S-NPP	Suomi NPOESS Preparatory Project
PAM	Precision Analog Monitor
PAT	Passive Analog Telemetry
PLO	Phase Locked Oscillator
PRT	Platinum Resistance Thermometer
QC	Quality Check
RC	Redundant Configuration
RDR	Raw Data Record
RF	Radio Frequency
RJ	Rayleigh-Jeans Approximation
RPS	Receiver Power Supply
SAW	Surface Acoustics Wave
SDE	Scan Drive Electronics
SDM	Scan Drive Mechanism
SN	Serial Number
SNO	Simultaneous Nadir Observation
SPA	Signal Processor Assembly
TVAC	Thermal Vacuum

APPENDIX

Appendix A ADDITIONAL INTRODUCTION

Appendix A contains additional information about QS ATMS

QS_ATMS_Additional_Information.pdf

Appendix B THE QS ATMS ANTENNA PATTERN COEFFICIENTS CORRECTION DATA

Appendix B contains relevant files of ATMS Antenna Pattern Coefficients data as provided below:

QS_ATMS_APCCoef.xlsx

Appendix C CALIBRATION ACCURACY DATA

Appendix C contains relevant files of instrument level TVAC calibration accuracy data prior to non-linearity correction as provided below:

CalAccuracyData(K).xlsx

Appendix D NON-LINEARITY DATA IN BRIGHTNESS TEMPERATURE

Appendix D contains relevant files of non-linearity brightness temperature data as provided below:

NonLinearityBrightnessTemp.xlsx

Appendix E NON-LINEARITY DATA IN RADIANCE

Appendix E contains relevant files of non-linearity radiance data as provided below:

NonLinearityRadiance.xlsx

Appendix F THE QS ATMS SPECTRAL RESPONSE FUNCTIONS DATA

Appendix F contains files of ATMS Spectral Response Functions (SRF) data and of the SRF processing note as provided below:

QS_ATMS_SRF.zip   QS ATMS SRF Public Release Announcemeı   QS_SRF_ProcessNote sWithMarchDataupda

Notes:

1. Data is presented in two columns: one for frequency in GHz and the other for amplitude in dB.
    a. All frequencies are in the radio frequency spectrum (they have been converted from intermediate frequencies, as applicable).
2. SRF amplitudes are normalized to the peak of the SRF. The peak of the normalized SRF is 0dB, and all other values will be less than that.
3. Two sets of data are provided based on whether ATMS is using the primary (PRI, also known as A-side) or redundant (RED, also known as B-side) local oscillator (LO) configuration. ATMS will be in primary LO configuration at launch.
4. CH1 and CH2 are direct detect and therefore do not have an LO. The channels 1 and 2 PRI files only.
5. Channels 3 through 22 have both PRI and RED files.
6. Data shown is for the nominal voltage and +20C measurements.